Aerospace Science and Technology 177 (2026) 112913

Contents lists available at ScienceDirect

Aerospace Science and Technology

journal homepage: www.elsevier.com/locate/aescte

An analysis of engine nacelle compartment leak and explosion hazards for a hydrogen-fuelled aircraft

Paul Holborn [a,*], Xiaoxiao Sun [a], Vishal Sethi [a], Michael Willmot [b]

[a] Faculty of Engineering and Applied Sciences, Cranfield University, Cranfield, Bedfordshire, MK43 0AL, UK
[b] Rolls-Royce plc, Kings Place, 3rd Floor 90 York Way, London, N1 9FX, UK

ARTICLE INFO

Editor: Cummings Russell

Keywords:
Hydrogen safety
Explosion hazard
Safety and certification
Aircraft engine
Nacelle compartment
Air ventilation
Computational fluid dynamics

ABSTRACT

The introduction of hydrogen as a fuel source in aircraft poses significant design and safety challenges, particularly regarding the consequences of hydrogen leaks in confined engine nacelle compartments. This study presents a detailed CFD-based analysis of hydrogen leak dispersion and explosion hazards in a simplified annular nacelle geometry, addressing a critical gap in aviation safety knowledge. STAR-CCM+ was used to simulate hydrogen dispersion, examining the influence of leak location, orientation, mass flow rate, and ventilation rate on the formation of flammable gas regions. FLACS-CFD was employed to predict explosion overpressures resulting from ignition of stoichiometric hydrogen-air mixtures. The work provides original contributions to hydrogen safety in aviation by quantifying tolerable leak limits and ventilation requirements, demonstrating that air-based ventilation alone may be insufficient for managing larger leaks. The results show that even small hydrogen leaks (> 0.1 g/s) can form flammable clouds capable of producing hazardous overpressures, especially under turbulent or congested conditions. Explosion simulations revealed that a 1 g stoichiometric (29.5% v/v) hydrogen-air cloud (occupying ~1% of the 3.8 m^3 compartment volume) can exceed tolerable overpressure thresholds (> 0.1 barg) unless large pressure relief vents are used. The potential impact of the findings is to offer guidance for the safety design, certification, and regulatory development of future hydrogen-fuelled aircraft engine powerplants.

1. Introduction

In order to meet internationally agreed commitments to reduce global CO_2 emissions by 2050, the aviation sector urgently needs to develop environmentally friendly alternatives to the traditional hydrocarbon-based fuels (kerosene - Jet A-1) that are currently used for aircraft. The use of hydrogen as an aviation fuel would eliminate in-flight CO_2 and other carbon-based emissions. Hydrogen propulsion has the potential to play a major part in reducing the climate impact and meeting the decarbonization targets of the aviation sector [1–13].

The usage of LH_2 as an aviation fuel will require the development of new types of aircraft design, fuel tanks and propulsion systems [14–17]. A key challenge that will need to be met in order to allow such a transition is the safety and certification of such systems [18–20]. Hydrogen has unique properties and behaves very differently to Jet A-1. Key differences, that need to be considered for safety and certification, include [21,22]:

- Leakage -hydrogen is a very small molecule with low viscosity. Consequently, small hydrogen leaks could occur relatively easily through imperfect seals, gaps or joins in the fuel system pipework or components. Jet A is far easier to contain.
- Flammable range – hydrogen has very wide flammability limits 4 - 74% at normal temperature and pressure (NTP) in comparison to Jet A-1 – and thus will form flammable gas mixtures over a much greater range, particularly if released in a confined or enclosed space. Jet A has a narrow flammable range and does not vaporise or generate flammable gas clouds to a significant degree at ambient temperatures.
- Very low minimum ignition energy (MIE) – hydrogen has an extremely low minimum ignition energy MIE – an order of magnitude less than kerosene for a stoichiometric fuel-air vapour mixture. Hence it can be ignited much more readily. In contrast Jet A contains additives that inhibit ignition and flame spread behaviour making it much easier to handle safety as an aircraft fuel.

* Corresponding author.
E-mail address: paul.holborn@cranfield.ac.uk (P. Holborn).

https://doi.org/10.1016/j.ast.2026.112913
Received 9 January 2026; Received in revised form 26 May 2026; Accepted 15 June 2026
Available online 16 June 2026
1270-9638/© 2026 The Authors. Published by Elsevier Masson SAS. This is an open access article under the CC BY license (http://creativecommons.org/licenses/by/4.0/).

- Buoyancy - At ambient temperatures hydrogen gas is extremely buoyant and will rise and disperse rapidly if released in an open environment. However, at very low temperatures of 22 K or less hydrogen has a density which is greater than that of air and hence under certain circumstances it also has the potential to behave as a dense gas.
- Burning behaviour – hydrogen is a more reactive gas with different combustion properties (higher burning velocity, heat of combustion and flame temperature) and radiative characteristics (low emissivity and radiative heat fraction) than Jet A.
- DDT behaviour – hydrogen has a much greater propensity to detonate and can undergo a DDT (deflagration to detonation transition) under a wide range of circumstances (e.g. congestion or confinement) and fuel-air mixture ratios producing a highly damaging detonation.
- Cryogenic liquid. Liquid hydrogen must be maintained at extremely low temperatures (20.4 K at atmospheric pressure) to be kept as a liquid. Above this temperature it will vaporise and boil vigorously releasing hydrogen gas.

1.1. Previous hydrogen aircraft safety studies and current knowledge gaps

A hazard analysis of hydrogen safety for hydrogen fuelled aircraft was carried out as part of the EU ENABLEH2 project [23–25]. The analysis identified the major hazards associated with both liquid and gaseous hydrogen systems for a variety of different aircraft architectures and leak scenarios. The implications of hydrogen hazard assessment and control for aircraft were examined, emphasising the need for a comprehensive safety framework to support the integration of liquid hydrogen (LH_2) propulsion systems in civil aviation. A Preliminary Hazard Analysis (PHA) and gap analysis were used to identify interconnected risks and missing knowledge. The key hazards identified include flammable atmosphere formation, ignition risks, cryogenic burns, explosion potential, and mechanical damage.

An FAA report [26] examined the hydrogen hazards associated with using hydrogen fuel cells (HFC) on-board aircraft (Appendix F) and suggested a recommended baseline for their regulation. One of the main findings was that air ventilation should be provided where hydrogen leakage into any compartment is a possibility. The report also concluded that hydrogen hazards were not well addressed in the current airworthiness requirements.

The EU HEAVEN project [27] carried out a successful flight demonstration of a LH_2 powered fuel cell propulsion aircraft, using a fuel tank storing 15 kg LH_2. A safety analysis of the aircraft was performed in accordance with ARP4761 guidelines for all flight phases. More than 250 potential failure scenarios and their mitigations were identified. Only a few were hazardous or catastrophic. On the basis of the safety analysis, it was concluded that the LH_2 tank and aircraft were safe to operate.

In December 2024, EASA (European Union Aviation Safety Authority) held an international workshop to develop a Hydrogen Certification Roadmap [19]. The workshop identified a number of key hazards and hydrogen safety research needs, including fire and explosion hazards within aircraft engine powerplants. Likewise, a complimentary FAA report [20] examines the development of a roadmap for safely enabling hydrogen-powered aircraft. Aviation safety research needs identified in the report included a recommendation that hydrogen fire and explosion characteristics need to be defined, and guidance materials developed for industry to certify hydrogen-combustion engine and propulsion system components.

The EU CONCERTO research project [28] has also recently highlighted gaps in the current European regulations for certification of a hydrogen-powered aircraft concerning missing or incomplete data for characterising hydrogen behaviour and critical areas for certification of hydrogen aircraft. One of the key knowledge gaps identified was the characterisation of hydrogen leaking and dispersion, build-up of flammable atmosphere, hazardous quantities and acceptable rates of leakage. Similarly, one of the main critical areas presenting the highest risks to certification for aircraft systems was found to be fire and explosion prevention and protection.

The UK CAA have also analysed EASA CS-25 [29] (the collection of airworthiness certification requirements that large aeroplanes must meet to conform to the safety objectives of European Law) with regards to the certification challenge of hydrogen powered aircraft and performed a gap analysis for hydrogen fuel systems [30]. The analysis identifies a number of hydrogen safety challenges in relation to venting and fire protection, fuel systems and emergency scenarios, and concludes that around 15% of requirements and 22% of AMCs (Acceptable Means of Compliance) would need to be revised.

One key area of concern is what the consequences of a hydrogen leak in the nacelle compartment of an aircraft engine powerplant might be and how any hazards arising from such a leak might be safely managed.

Although some previous research studies have considered the safety implications of using hydrogen as a fuel for stationary gas turbine enclosures [31], aircraft nacelle compartments differ markedly in geometry, ventilation, and operating environment. Aircraft nacelles are compact, aerodynamically constrained structures with minimal free volume, tightly conforming to the engine layout to reduce weight and drag, whereas stationary enclosures are typically much larger, room-like housings designed for accessibility, maintenance, and hazard management. Ventilation in nacelles must flow through limited inlets, vents, and exhaust paths while stationary enclosures use actively controlled, forced ventilation systems sized for heat removal and gas dilution. Nacelles also operate in a highly variable environment over a wide range of ambient pressure, temperature, and engine operating conditions, including take-off, cruise and shutdown, whereas stationary enclosures usually operate in a near-ground, relatively steady ambient environment.

By addressing this knowledge gap and, for the first time, characterising hydrogen leak and explosion behaviour and determining hazardous quantities and acceptable rates of leakage for a nacelle compartment, the research presented in this paper provides an original contribution to knowledge, beyond the current state-of-the-art.

1.2. The aircraft engine nacelle compartment

Fig. 1 shows the two different types of compartment that are typically found in an aircraft turbofan engine nacelle. These are:

(i) The nacelle compartment (zone 1)

The nacelle compartment (also known as the cowl compartment, cowl cavity, fan compartment or accessory zone) is an annular region located between the engine fan case and outer cowl and forward and aft bulkheads. It is denoted by the blue hatched region shown in Fig. 1.1. In a kerosene fuelled aircraft engine, the nacelle compartment usually contains an accessory gearbox and a significant amount of pipework and other congestion. Air ventilation is used to cool the compartment and purge any vapours, should a fuel leak occur, to prevent a flammable atmosphere from forming inside the compartment. There is also usually a drainage hole located at the bottom of the nacelle compartment, to allow any liquid fuel to drain away and prevent it accumulating inside the compartment.

(ii)The core compartment (zone 2)

The core compartment is an inner annular region located around the engine core (denoted by the red hatched region shown in Fig. 1). It contains systems to support combustion and allow airflow cooling of the turbofan engine core.

A nacelle compartment in a traditional kerosene fuelled aircraft engine is designed to be resilient to the consequences of the hazards that

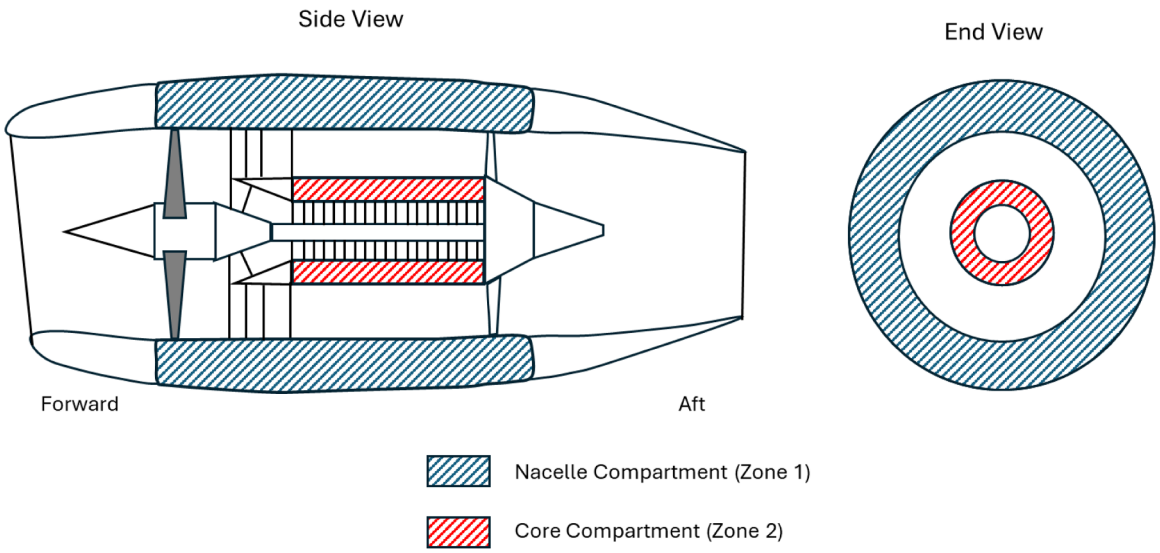


Fig. 1. The types of compartment found in an aircraft turbofan engine powerplant.

are likely to occur in practice (mostly fire). In the event of a fuel leak it should be able to continue operating or be safely shutdown. This approach has been borne out by operating flight experience on civil aircraft over the last 70 years. However, such an approach is likely to be more difficult to achieve with hydrogen since leaks are already in a gaseous state (or will readily vaporise if leaking as LH_2) rather than as a liquid, as is the case with kerosene.

This paper describes how CFD modelling has been applied to examine the dispersion and explosion behaviour of hydrogen leaks in a simplified annular nacelle compartment (zone 1) geometry. The Siemens' STAR-CCM+ code has been used to simulate hydrogen leak dispersion and the effect of controlling parameters, including leak location, orientation, mass flow rate and ventilation airflow rate, on the size of the flammable region formed in a nacelle compartment. Similarly, the FLACS-CFD code has also been employed to predict the magnitude of the explosion overpressures for ignition of characteristic flammable hydrogen mixtures in a nacelle compartment.

The analysis provides information about safe ventilation, prevention of hazardous accumulation, and analysis of explosion risks in a designated fire zone. As such it supports proposed CS-25 [29] amendments, AMCs, and certification review items, such as those identified in the CAA report [30], to aid with the development of a hydrogen-specific special condition. The research can help address unmet technical and safety requirements with regards to:

CS 25.1193 (Cowling and Nacelle skin) which must meet the requirements of CS 25.1187 (Drainage and ventilation of fire zones) where no hydrogen-specific ventilation/management guidance currently exists.
CS 25.1189 (Shut-off means) and AMC 25.1189 (Determining hazardous quantity of flammable fluids) - where it can inform development of a new AMC for controlling fire and explosion hazards as to the acceptable/tolerable amount of hydrogen leakage into a nacelle compartment.

The results of the analysis have been used to indicate the level of hydrogen leakage that could be safely managed/tolerated using air ventilation in terms of the size (mass/volume) of the flammable gas region formed inside the compartment using air ventilation alone. Hence, they can help to inform safety design and certification of future hydrogen fuelled engine powerplants.

2. Method

The dispersion behaviour of hydrogen leaks into a simplified nacelle compartment geometry was simulated using the Siemens' STAR-CCM+ (version 19.02.013) code [32]. The FLACS-CFD code (v22.2) [33] was used to simulate the explosion behaviour of flammable hydrogen clouds in a simplified engine nacelle compartment geometry.

STAR-CCM+ was selected for modelling hydrogen leak dispersion behaviour, since it provides high-fidelity CFD capabilities with advanced turbulence models for accurately capturing the behaviour of hydrogen as it disperses in air and can represent complex geometries and boundary conditions allowing detailed modelling of leak scenarios in enclosures. FLACS-CFD was selected for modelling the explosion behaviour in the nacelle compartment since it is an explosion-focused solver, specifically designed for modelling gas explosions, deflagrations, and blast wave propagation in complex geometries that is able to efficiently obtain solutions for hydrogen safety engineering explosion scenarios.

In the conceptual aircraft fuel system being examined in this paper, hydrogen will be stored as LH_2 in the fuel tank but then converted into GH_2 and heated (via a heat exchanger) while being pumped at high pressure (at around 70 barg) and transported to the engine nacelle compartment where it will then be injected into the engine core combustor. The analysis presented here therefore focuses primarily on gaseous hydrogen leak hazards inside the engine nacelle compartment, assuming that any LH_2 from the fuel tank is converted into gaseous H_2 prior to entering the nacelle compartment, where it has reached a temperature of 288 K. For alternative fuel system designs where LH_2 is used directly in the nacelle compartment additional complexities and hydrogen hazards will arise as discussed in Section 5.4.

2.1. CFD modelling of hydrogen leak dispersion behaviour using STAR-CCM+

STAR-CCM+ is a fundamental CFD code solving the conservation equations for mass, momentum, energy and species transport. A selection of turbulence models is available to predict turbulent fluid flow. Gas properties for hydrogen and air were selected from the STAR-CCM+ database. The compartment geometry used in the STAR-CCM+ simulations was defined using the SolidWorks CAD software and then imported. STAR-CCM+ allows the use of an unstructured grid which can be

applied to simulate complex geometries in a flexible and efficient way. The STAR-CCM+ simulations were performed using Cranfield University's High-Performance Computing (HPC) facility employing up to 256 cores.

2.2. Notional nozzle theory

Notional nozzle theory was used to calculate the expanded hydrogen leak diameter used in the STAR-CCM+ hydrogen dispersion simulations. At typical pressures used in applications (i.e. where the ratio of the supply pressure to the ambient pressure > 1.89) a hydrogen leak will be underexpanded and choked at the nozzle exit. Upon release, such choked flows exhibit complex shock behaviour at the exit hole, requiring a very fine grid and significant computational resources to simulate. An alternative approach, that is commonly adopted to model hydrogen leaks, is to employ what is known as notional nozzle or pseudo source theory [34]. Notional nozzle theory assumes that the leak from the actual leak orifice can be effectively treated as if it is released from a larger notional nozzle diameter where the hydrogen leak has fully expanded to atmospheric pressure. This means that the hydrogen leak can then be modelled directly, without the need to resolve the complex shock behaviour produced at the actual nozzle exit. The size of the notional nozzle diameter that is required can be obtained by solving the conservation equations at the real and notional nozzle exit. Several different pseudo source modelling approaches for achieving this have been developed, differing in the assumptions that are made and conservation equations that are employed [35]. The Ewan/Moodie notional nozzle model [36] was used in this study

Justification for the applicability of the Ewan/Moodie notional nozzle theory to high-pressure hydrogen leakage scenarios is given in the study by Velikorodny and Kudriakov [37], who performed simulations of highly underexpanded (high pressure) gas jets validated against several experimental data sources available in the literature. The Ewan/Moodie notional nozzle model was shown to perform well for high-pressure turbulent hydrogen/helium gas leaks and provided a better fit to the available experimental data than either the Birch or Yuceil and Otugen notional nozzle models.

2.3. The FLACS-CFD model

FLACS-CFD was originally developed in the 1980 and 90s for use in the Oil and Gas industry. It provides capabilities for carrying out safety studies by simulating accident scenarios involving fluid flow behaviour in complex 3D geometries by modelling flammable gas hazard effects such as gas explosions and blast waves. FLACS-CFD is a structured Cartesian grid, finite volume CFD code. The code solves the compressible conservation equations for mass, momentum, enthalpy, mass fraction of chemical species, turbulent kinetic energy and dissipation rate of turbulent kinetic energy [33]. The numerical treatment used in the FLACS-CFD solver employs a second order scheme in space, and a first/second order in time. The pressure and velocity fields are coupled via the SIMPLE solution algorithm [38]. A standard k-ε turbulence model is also utilised incorporating modifications for generation of turbulence behind sub-grid obstacles and turbulent wall functions.

FLACS-CFD employs the Porosity/Distributed Resistance method to model the turbulence generated by subgrid scale objects [33]. This allows for the efficient simulation of gas dispersion behaviour in complex geometries using relatively coarse numerical grids.

The convergence of solutions in FLACS is managed through the Courant-Friedrich-Levy (CFL) number [33]. An adaptive time step routine is used, with the time step adjusted to meet CFL number stability criteria based upon both the speed of sound (CFLC) and the fluid flow velocity (CFLV). Each time step length is selected so that both sound waves and the fluid may propagate only a limited distance, equal to the average control volume length multiplied by the CFLC/CFLV number.

In order to model explosion behaviour FLACS employs a combustion model [33]. This is comprised of a flame model and a burning velocity model. A one-step reaction kinetic model is assumed with the rate of reaction determined by the burning velocity of the fuel mixture. A chemical equilibrium model is used to estimate the composition of the combustion products. In most practical engineering simulations, the flame reaction zone is typically thin compared to the grid resolution. To overcome this problem, in the β flame model employed in FLACS, the flame is artificially thickened so that its structure may be fully resolved by a relatively coarse grid. The flame zone is thickened by increasing the diffusion coefficient by a factor β and reducing the reaction rate by a factor $1/\beta$. The factor β used to achieve this is proportional to the grid size and inversely proportional to the integral length scale, giving the flame a constant thickness equal to 3-5 grid cells and guarantying that the flame propagates with the specified burning velocity.

The burning velocity model comprises three sub-models with burning velocities corresponding to the laminar, quasi-laminar and turbulent combustion regimes. The FLACS code switches the value of the effective burning velocity used in the model depending upon the relative magnitude of these three burning velocities. In the *laminar combustion regime* (typically close to the ignition source) the flame front is assumed to be smooth and the burning velocity is calculated using a look-up table where it is expressed as a polynomial function of the equivalence ratio and flammability limits (fitted to empirical data obtained for laminar premixed hydrogen-air flames). The flammability limits of hydrogen-air mixtures are used in FLACS to prevent flame propagation when the concentration is above the upper limit (75%) or below the lower limit (4%). Thus, if there are regions above 75% hydrogen in air at the point of ignition, the flame will not propagate and ignition will fail. As the flame propagates further away from the ignition source it begins to deform and wrinkle due to the effect of flame instabilities (e.g. Rayleigh-Taylor and thermal diffusive) resulting in an increase in the burning velocity. Finally, in the *turbulent combustion regime* the turbulent burning velocity is expressed as a function of the turbulent flow intensity and length scale – based upon experimental data obtained by Abdel-Gayed *et* al [39].

The FLACS explosion model has been validated against a wide range of experiments (at small, medium and large scale) and has received specific validation for simulating hydrogen-air dispersion and explosion behaviour [40–51]. The predictive performance is deemed to be relatively good, although there is a spread of results and the uncertainty in the predicted overpressures may be significantly higher or lower than observed values (by a factor of 2 or more) [33].

2.4. Annular nacelle compartment geometry

In the FLACS-CFD modelling work, the engine nacelle cowl compartment was also represented as the annulus formed between an inner and outer cylinder (see Fig. 4.4). This was achieved in FLACS by subtracting the inner cylinder from the outer cylinder using a "left difference" operation. The diameter of the inner cylinder, D_1 was 1.3 m, while the outer cylinder D_2 was 1.9 m. The length of the annulus, L, was set to 2.5 m giving an internal volume of 3.8 m^3. The annulus was also capped at either end to form the compartment forward and aft bulkhead walls. A vent opening, 0.2 m x 0.4 m (L x W), was introduced into the outer cylinder wall of the annulus at the aft end of the compartment. The geometrical objects defined in FLACS-CFD were mapped on to the underlying numerical grid specified for a given simulation. These were used to generate a porosity for each grid cell. The aggregate result is a porosity region that will approximate the annular nacelle compartment used in the simulation.

3. Dispersion simulations of a hydrogen leak in a nacelle compartment

A series of CFD simulations were performed using the Star CCM+ code to examine the behaviour of hydrogen jet leaks in an annular nacelle compartment geometry.

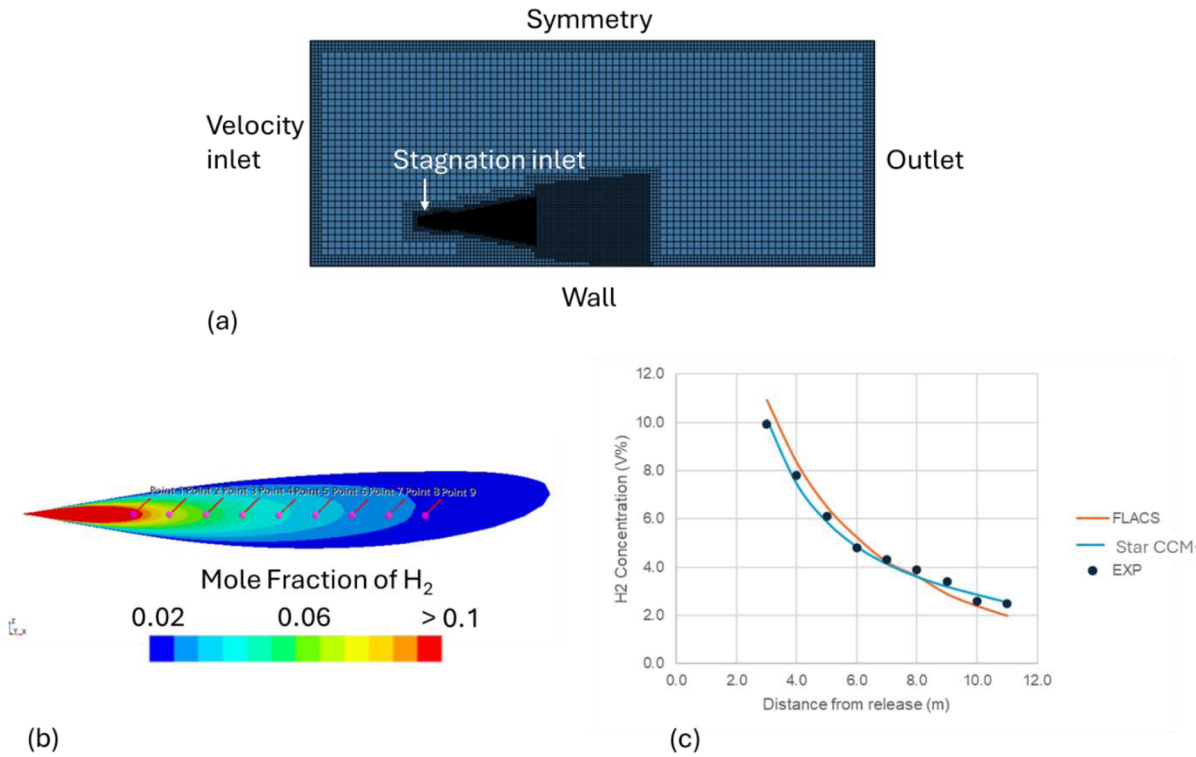


Fig. 2. The simulation results obtained using Star CCM+ for validation case 2: (a): numerical mesh used in the simulation (b) 2D contour plot of predicted hydrogen concentrations produced by the leak; (c) comparison of the STAR-CCM+ predicted H_2 concentration results with experimental test data [52] and results obtained using FLACS-CFD.

3.1. Initial validation

Star CCM+ has not previously received the same level of validation against experimental test data for hydrogen as has FLACS-CFD. To establish confidence in the code's predictions for hydrogen dispersion behaviour, an initial validation study comparing the predictions of Star-CCM+ with a suitable experimental test case was conducted. Roberts *et* al [52] performed a series of experimental tests for high stagnation pressure hydrogen leaks at atmospheric pressure and temperature. Test 7, with a leak at 100 bara through a 3 mm diameter leak hole (mass flow rate 0.045 kg/s), producing a sonic hydrogen jet (momentum effects dominate), was selected for comparison. The hydrogen concentration was monitored at several locations (at a height of 1.5 m) downstream of the leak and averaged over a period of 50s (for this test fluctuations of wind direction and speed had only a minor effect).

A model was set up using Star CCM+ to simulate the steady-state dispersion behaviour of the hydrogen leak for this validation case. A numerical domain 25 m x 10 m x 10 m was used. Fig. 2 (a) shows the grid employed in the simulation. A highly refined grid region was defined downstream of the leak outlet to capture the detailed behaviour of the plume. Outside of the high-definition region, the grid size was expanded as successively coarser meshes were defined towards the boundaries of the domain. Further refining the mesh did not modify the results obtained. The total number of grid cells used in the simulation was 4.3 million. The hydrogen leak was represented as a stagnation inlet. The boundary opposite the leak was defined as an outlet, while the boundary upstream of the leak was defined as a velocity inlet. The ground was defined as a wall, and the remaining side and top boundaries were defined as symmetry boundary conditions. The RANS RKE turbulence model was used. Gravity effect was set to be "on", and the coupled implicit solver was employed. To obtain a converged solution it was required that the residuals dropped by at least 3 orders of magnitude and that the flow parameters monitored reached a steady-state value.

Fig. 2 (b) shows a 2D contour plot of the hydrogen concentrations predicted. In this case momentum dominates over buoyancy and the plume is effectively horizontal. The hydrogen concentrations predicted by the Star CCM+ model (blue line) are in good agreement with the experimental test data (solid dots) as shown in Fig. 2 (c).

3.2. Model configuration

Having validated the predictions of Star CCM+ against experimental hydrogen dispersion data, the code was then applied to model hydrogen leak dispersion behaviour in an annular nacelle geometry. A schematic diagram of the simplified annular nacelle compartment model geometry used in the simulations is shown in Fig. 3. The model consists of an annular space formed between inner and outer cylinders and capped at either end by forward and aft bulkheads. Air flows into the compartment from a ventilation inlet that is assumed to cover the annular area at the forward end of the compartment. Hydrogen gas leaks into the compartment from an inlet with a specified mass flow rate, location and direction. The hydrogen then mixes with the ventilation air and the hydrogen-air gas mixture formed is vented through an opening located at the top of the compartment. The scenario modelled also assumes that the hydrogen leak in the nacelle compartment occurs whilst at sea level static, under max take off operating conditions (assumed as a worst-case hydrogen leak scenario) at an ambient temperature and pressure of 288 K and 101,325 Pa.

The simplified annular nacelle cowl compartment model used the dimensions specified in Table 1.

The gas dispersion behaviour produced in the nacelle compartment was represented as an internal flow only. Hence, the external gas dispersion behaviour at the vent, outside the nacelle compartment and outer bounding wall thickness of the nacelle cowl wall were not included in the model.

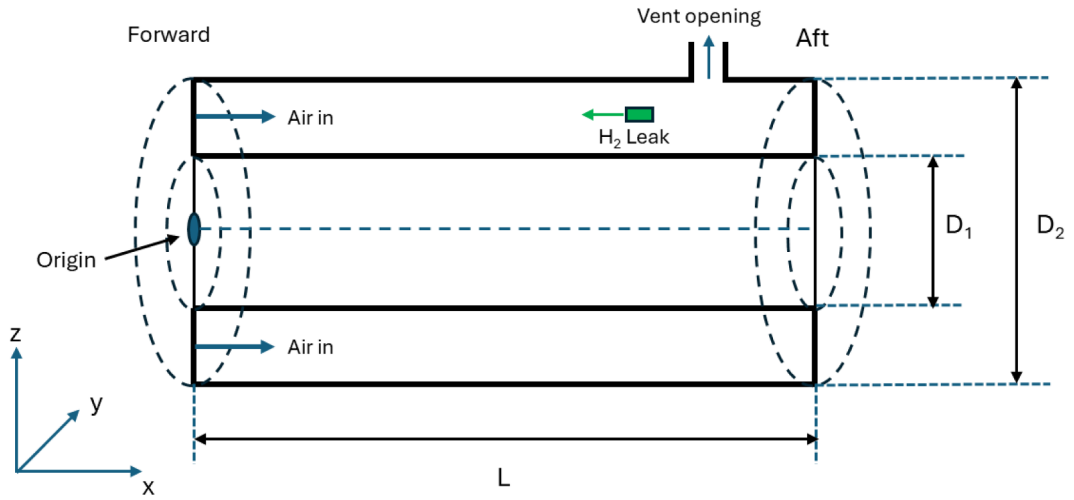


Fig. 3. Schematic diagram of the simplified annular nacelle compartment geometry.

Table 1
The dimensions of the annular nacelle compartment used in the model.

Dimension	Value
Inner diameter, D_1	1.3 m
Outer diameter, D_2	1.9 m
Compartment length, L	2.5 m

3.3. Hydrogen leak

Hydrogen jet leaks in the compartment were assumed to occur from a hole in a pressurised fuel pipe at 70 barg and 288 K (see Section 2). A series of different hydrogen mass leak rates were specified, and notional nozzle theory was used to obtain the effective leak diameter (and area) for an under-expanded jet leak once it had expanded to atmospheric pressure, as shown in Table 2.

The relative turbulence intensity used was 10% (intended to characterise a relatively high level of turbulence) and the turbulent length scale was set equal to the notional nozzle diameter found for each leak size (to provide a suitable characteristic length scale). The hydrogen leak was represented as a mass inlet boundary condition. In order to produce a suitable boundary in the model geometry a small cylinder with the same diameter as the notional nozzle, positioned at an appropriate orientation to match the direction of the hydrogen leak, was cut out of the domain.

3.4. Air ventilation inlet

Air ventilation into the compartment was assumed to be at a specified rate of air changes per minute (ACM) entering across the free annular area at the forward end of the compartment. The air mass flow rate (kg/s) into the nacelle compartment was calculated using:

$$\dot{m}_{air} = \frac{n_{air}\ V_c}{60}\left(\frac{p_{air} W_{air}}{R_u T_{air}}\right) \quad (1)$$

where n_{air} is the number of air changes per minute specified for the nacelle compartment, V_c is the compartment volume (m^3), p_{air} is the ambient air pressure (Pa), T_{air} is the ambient air temperature (K), R_u is the universal gas constant (J/mol/K) and W_{air} is the molecular mass of air (kg/mol). With 5 air changes per minute for ambient air at pressure of 101,325 Pa and temperature 288 K, for the annular compartment volume of 3.8 m^3, the corresponding air mass flow rate is 0.3850 kg/s (while for 2.5 ACM it is 0.1925 kg/s and for 10 ACM it is 0.77 kg/s). The air inlet was represented in the simulation as a mass inlet boundary condition.

Table 2
The effective area and diameter of the hydrogen leaks used in the simulations, obtained using notional nozzle theory.

H_2 leak rate (g/s)	Notional nozzle area (m^2)	Notional nozzle diameter (mm)
0.1	8.2592E-07	1.03
0.5	4.1296E-06	2.29
1	8.2592E-06	3.24
2	1.6518E-05	4.59
5	4.1296E-05	7.25
10	8.2592E-05	10.25

3.5. Ventilation outlet

The hydrogen-air gas mixture formed by the leak mixing with the air exits through a cuboidal exhaust chimney outlet of specified area (length, Δx, and width, Δy) positioned at the top of the compartment with the vent centre located at (2.3, 0, 0.95). The height of the exhaust chimney box was set to 0.4 m. The vent opening was represented in the simulation as a pressure outlet at the top of the chimney.

3.6. Hydrogen leak dispersion simulations

The steady-state solver was used to find the equilibrium solution for the hydrogen concentration distribution, pressure and gas velocity flow field in the compartment. Simulations were carried out to determine the effect of selected parameters on the spatial distribution of hydrogen concentration and the extent of the flammable zone formed in the nacelle cavity. The matrix of simulation runs that were performed is given in Table 3.

The model was initially set up for the base case scenario, Run A1, for a 1 g/s leak that flows horizontally in the "-X" direction towards the forward end of the compartment. The boundary conditions assigned are given in Table 4.

Fig. 4 (a) shows an example of the grid employed in the simulation work. A highly refined grid region was defined downstream of the leak outlet in order to capture the detailed behaviour of the plume. Outside of the high-definition region, the grid size was expanded as successively coarser meshes were defined towards the boundaries of the domain.

A higher grid refinement was also used around the exhaust chimney vent outlet. A grid independence study was then performed for the base

Table 3
The matrix of steady-state simulation runs performed for hydrogen leaks in the simplified annular nacelle compartment geometry using Star CCM+.

Run	H_2 leak rate (g/s)	Leak location (m)	Leak direction	Air ventilation
A1	1	(2.05, 0, 0.8)	"-X"	5 ACM
A2	1	(2.05, 0, 0.8)	"+Y"	5 ACM
A3	1	(2.05, 0, 0.66)	"+Z"	5 ACM
A4	1	(0.45, 0, 0.8)	"+X"	5 ACM
A5	1	(2.05, 0.8, 0.)	"-X"	5 ACM
A6	1	(2.05, 0.66, 0.)	"+Y"	5 ACM
A7	1	(2.05, 0.8, 0.)	"+Z"	5 ACM
A8	1	(2.05, 0, 0.8)	"+X"	5 ACM
A12	1	(2.05, 0, 0.8)	"-X"	2.5 ACM
A13	1	(2.05, 0, 0.8)	"-X"	10 ACM
A14	0.1	(2.05, 0, 0.8)	"-X"	5 ACM
A15	0.5	(2.05, 0, 0.8)	"-X"	5 ACM
A16	2	(2.05, 0, 0.8)	"-X"	5 ACM
A17	5	(2.05, 0, 0.8)	"-X"	5 ACM
A18	10	(2.05, 0, 0.8)	"-X"	5 ACM

Table 4
The boundary conditions used in the simulations.

Boundaries	Set up	Value
Air inlet	Mass flow inlet	0.385kg/s (5 ACM)
H_2 inlet	Velocity inlet	1085m/s (1 g/s)
Vent outlet	Pressure outlet	0 Pa
Walls	Adiabatic	N/A

case Run A1 to test the sensitivity of the predicted hydrogen concentration results to the number of grid cells used. The results, shown in Fig. 4 (b), suggest that a reasonable level of grid independence is achieved when using around 8 million cells, producing very similar results to the simulation employing 33 million cells. The total number of cells used for the remaining simulations was therefore limited to around 10 million cells. The grid cell size used in the nacelle compartment varied from 0.25 mm to 20 mm.

3.7. Results

The results obtained for each run case in the matrix were visualised using both a 2-D x-z contour plane (located at y = 0) showing the distribution of hydrogen concentrations at the top of the compartment, and a 3-D iso-surface showing the location of the 4% v/v LFL within the annular nacelle compartment.

Fig. 5 (a) shows the hydrogen concentration results obtained for the base case, Run A1. The hydrogen plume formed projects horizontally along the top of the compartment from the leak hole in the "-X" direction towards the forward part of the compartment. High concentrations are predicted close to the leak point and decrease towards the front. The 3D LFL iso-surface reveals a symmetric structure, with the flammable region running horizontally from the leak position along the upper part of the compartment towards the front, before forming into two symmetric lobes positioned either side of the centre projecting downwards and back along the sides of the compartment. The total mass of hydrogen in the compartment for Run A1 is calculated to be 8.55 g. The results

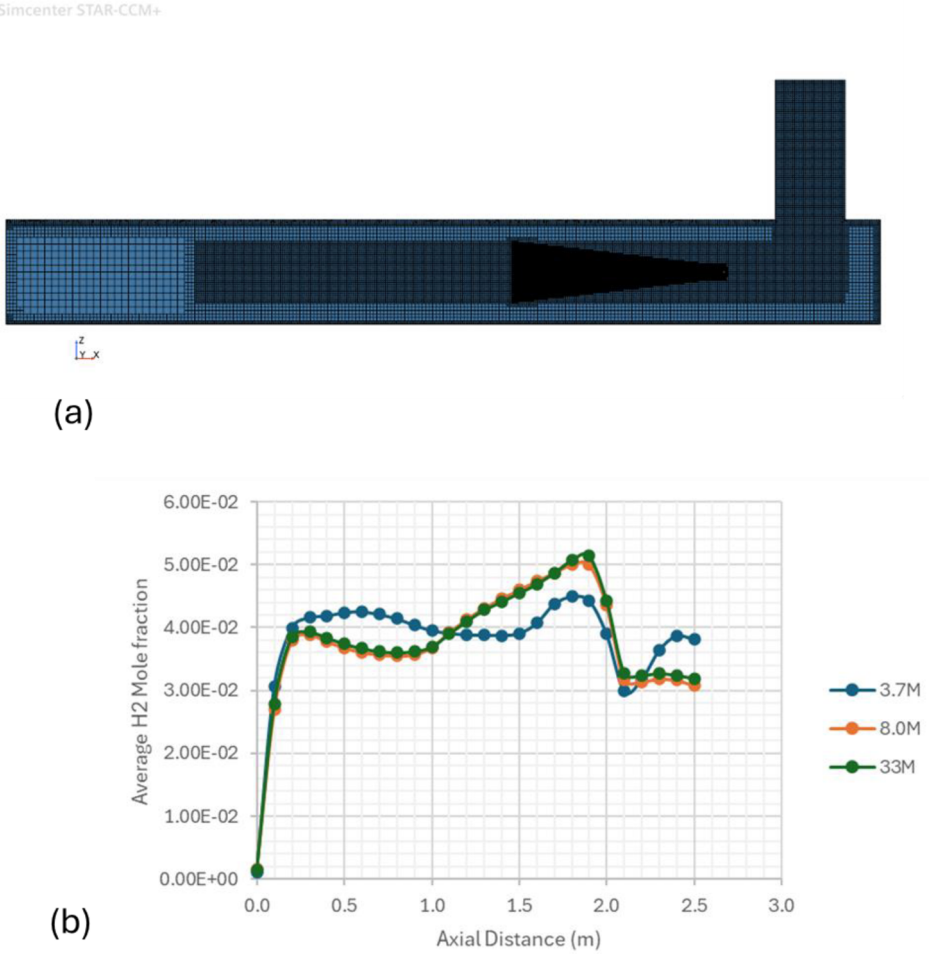


Fig. 4. (a) The numerical grid used in the simulation of the annular nacelle compartment for case Run A1; (b) the results of the grid sensitivity study, suggesting that grid independence is achieved when using around 8 million cells.

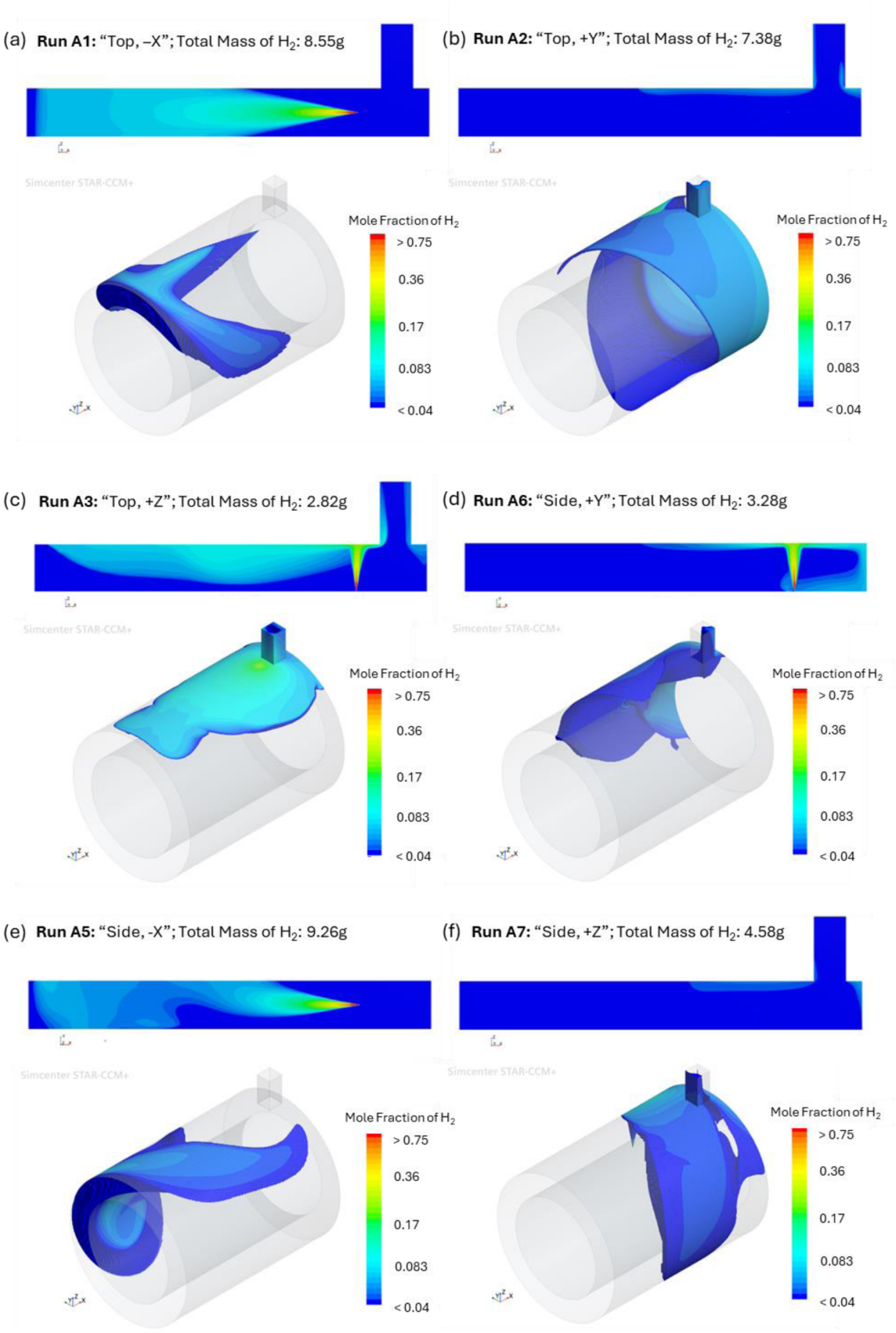


Fig. 5. Simulation results showing the effect of varying the location and orientation of a 1 g/s hydrogen leak on the flammable gas cloud formed in the nacelle compartment.

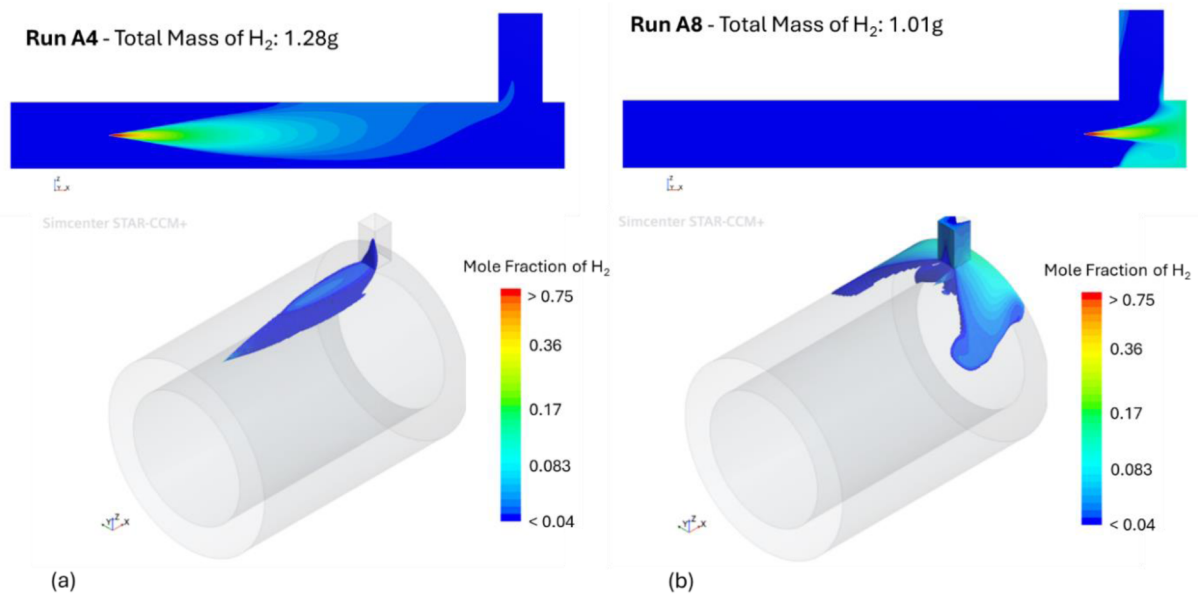


Fig. 6. Simulation results for: (a) Run A4, a 1 g/s H_2 leak, at the top (forward end), in the "+X" direction; (b) Run A8, a 1 g/s H_2 leak, at the top (aft end), in the "+X" direction.

obtained for Run A2, shifting the orientation of the leak to run in the "+Y" direction are shown in Fig. 5 (b). In this case the LFL iso-surface forms a layer that wraps completely around the circumference of the aft part of the compartment. The mass of hydrogen in this case is 7.38 g. Fig. 5 (c) shows the hydrogen leak distribution produced for Run A3, an upward "+Z" leak located at the top of the compartment. The hydrogen forms an upward plume that forms a layer beneath the top of the compartment. The LFL region is likewise concentrated under the top of the compartment. The flammable mass of hydrogen in the compartment, at 2.82 g, is around a third of that predicted for the base case Run A1. This is a consequence of the upwards directed leak being in close proximity to the ventilation outlet, resulting in a significant fraction of the hydrogen exiting directly through the outlet rather than accumulating within the compartment. Fig. 5 (d) shows the results obtained for Run A6 with a "+Y" directed leak located at the side of the compartment. In this case the hydrogen plume and layer are formed along the aft end of one side of the compartment. Once again much of the hydrogen exits directly through the outlet producing a relatively low flammable mass of 3.28 g. Fig. 5 (e) shows the results obtained for Run A5 with a forward facing "-X" leak located at the side of the compartment. The hydrogen travels forward along the side of the compartment before circulating around back along the top of the opposite side. In this case, because the circulation pattern is directed away from the vent outlet the flammable mass in the compartment is 9.26 g, higher than the base case. The results obtained for Run A7, with an upward "+Z" leak located at the side of the compartment are shown in Fig. 5 (f). The LFL

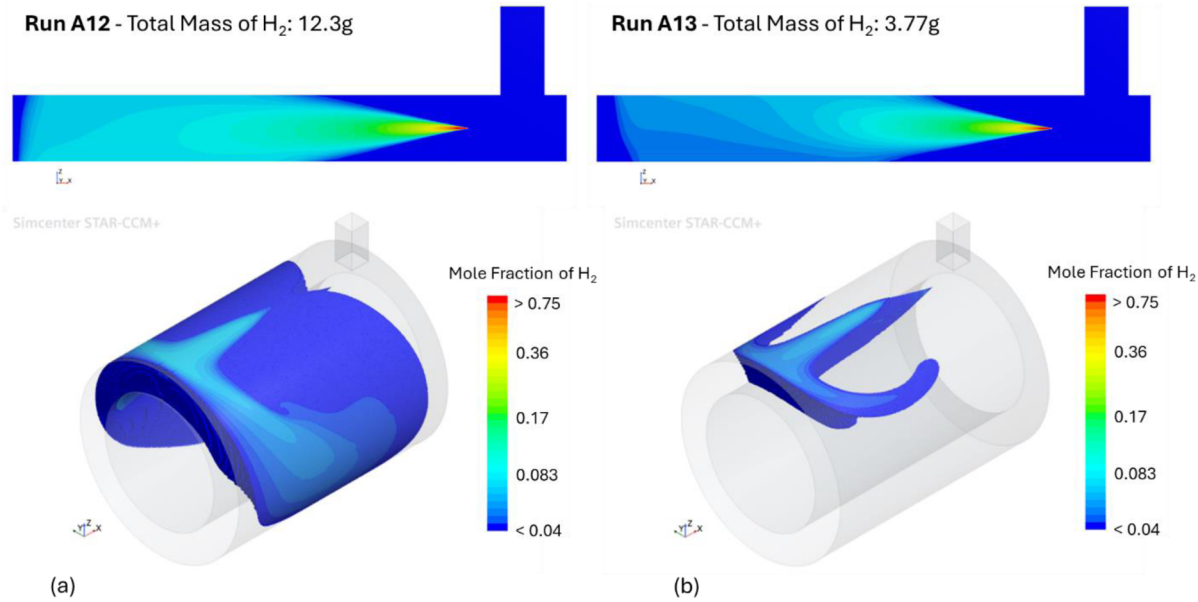


Fig. 7. Simulation results for: (a) Run A12, a 1 g/s H_2 leak, at the top, in the "-X" direction, at 2.5 ACM; (b) Run A13, a 1 g/s H_2 leak, at the top, in the "-X" direction, at 10 ACM.

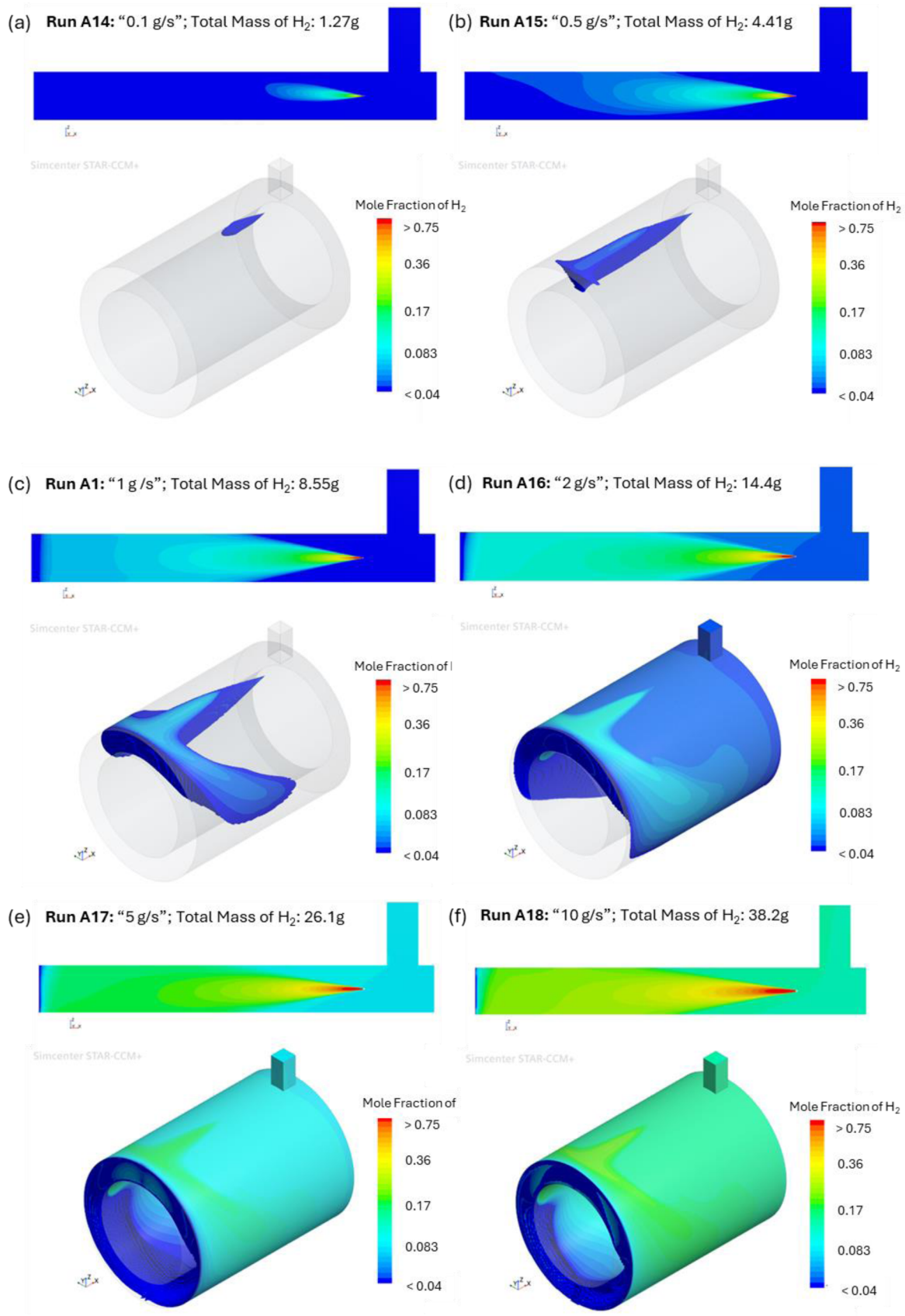


Fig. 8. Simulations results for different hydrogen leak rates into the nacelle compartment: (a) 0.1 g/s; (b) 0.5 g/s; (c) 1.0 g/s; (d) 2 g/s and (e) 5 g/s.

Table 5
The size of the equivalent stoichiometric cloud formed in the nacelle compartment for different hydrogen leak rates.

Hydrogen leak rate (g/s)	Total mass of hydrogen in compartment (g)	Equivalent stoichiometric cloud (m^3)
0.1	1.27	0.05
0.5	4.41	0.17
1.0	8.55	0.34
2.0	14.4	0.56
5.0	26.1	1.02

iso-surface forms a layer at the top that wraps around to the opposite side in the aft part of the compartment. The proximity of the vent outlet reduces the flammable mass to 4.58 g.

Fig. 6 (a) shows the results obtained for Run A4, with a "+X" leak located at the top of the compartment and also moved forward. In this case the hydrogen plume and LFL region runs horizontally along the top of the compartment before exiting directly through the outlet. The flammable mass predicted in the compartment is only 1.28 g, 15% of that for Run A1. For Run A8, shown in Fig. 8 (b), the leak is located at the same position as for the base case Run A1 but directed in the "+X" rather than the "-X" direction. The release forms two symmetric lobes at the aft end of the compartment positioned either side of the centre projecting downwards. Once again, the close proximity of the vent outlet to the leak results in a significantly lower flammable mass in the compartment of 1.01 g.

Runs A12 and A13 respectively half and double the air ventilation rate in compartment for Run A1 to 2.5 and 10 ACM. The results are shown in Fig. 7 (a-b). The qualitative form of the hydrogen plume and LFL iso-surface in the compartment remains the same but the extent of the region is increased at 2.5 ACM or decreased at 10 ACM. Likewise, the flammable mass in the compartment is respectively increased to 12.3 g or reduced to 3.77 g.

Runs A14 to 18 were used to examine the effect of increasing the mass leak rate of hydrogen into the compartment from 0.1 g/s to 10 g/s. The results are shown in Fig. 8 as the leak rate increases the extent of the plume and LFL iso surface in the compartment also grows from just a small region at the top of the compartment to filling the entire compartment (Fig. 8 (e), Run A17, 5 g/s) and then with increasing concentration throughout the compartment. Likewise, the predicted total mass of hydrogen in the compartment increases from 1.27 g (Fig. 8 (a), Run A14, 0.1 g/s) to 38.2 g (Fig. 8 (f), Run A18, 10 g/s).

The masses of hydrogen predicted for each of the runs in Table 5 were also used to estimate the size of the equivalent stoichiometric cloud (i.e. the volume of the uniform stoichiometric hydrogen-air cloud that contains the same total mass of hydrogen) formed in the nacelle compartment, as shown in Table 5. Note that the volume of the cloud predicted using the total mass of hydrogen in the compartment is expected to be pessimistic since it will overestimate the amount of hydrogen falling in the flammable range.

At a leak rate of 0.1 g/s, the total mass of hydrogen predicted in the compartment is 1.27 g and the volume of the equivalent stoichiometric cloud produced in the compartment is around 0.05 m^3. As the leak rate increases the size of the equivalent cloud also increases significantly. For a leak rate of 5 g/s the equivalent stoichiometric cloud volume is around 1 m^3.

4. Explosion simulations of hydrogen clouds in a nacelle compartment

If a hydrogen gas leak into an engine nacelle compartment should occur the question arises as to what amount (volume/mass) of flammable hydrogen cloud in the compartment could be deemed acceptable or tolerable? To try to address this question and gauge the size of flammable gas cloud from a hydrogen gas leak into the nacelle compartment that could be tolerated, FLACS-CFD was used to simulate the gas explosion overpressure that would be generated by the ignition of a small stoichiometric hydrogen-air cloud volume located in the simplified annular nacelle compartment geometry.

4.1. Model setup

The explosion simulations for the annular nacelle compartment geometry were performed in accordance with FLACS Best Practice Guidelines [33].

Based on the dispersion simulation performed in Section 3, a stoichiometric (29.5% v/v) hydrogen-air cloud having a volume of 0.45 m x 0.3 m x 0.3 m (0.0405 m^3) was defined in the annular nacelle compartment (Fig. 9). Such a cloud occupies around 1% of total annular compartment volume of 3.8 m^3 and contains a mass of around 1 g of hydrogen (corresponding to a hydrogen leak rate of around 0.1 g/s – see Table 5).

A series of simulations were performed to examine the effect on the peak gas explosion overpressure generated inside the compartment of:

- pressure relief vent area
- initial gas cloud turbulence level (quiescent/highly turbulent)
- location of the gas cloud within compartment
- pipework congestion within cloud

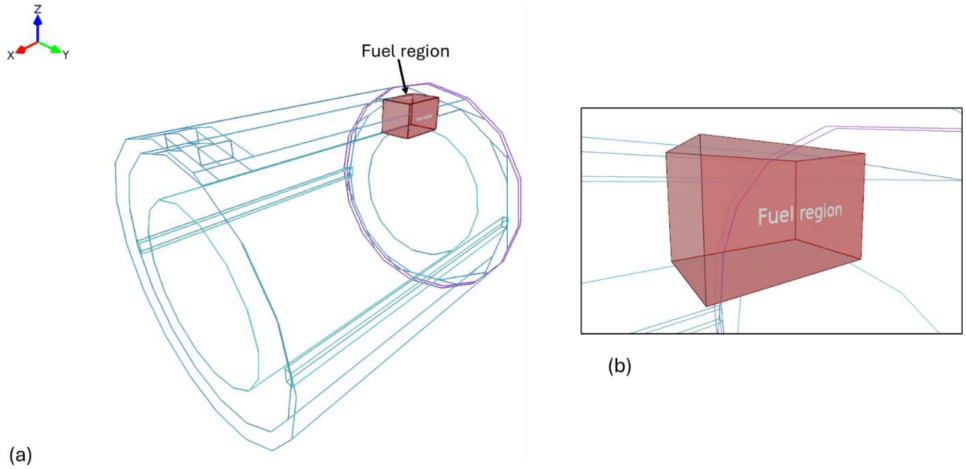


Fig. 9. The small stoichiometric H_2-air cloud volume used in the explosion simulations: (a) location of the cloud in the annular nacelle compartment; (b) a magnified view of fuel cloud region.

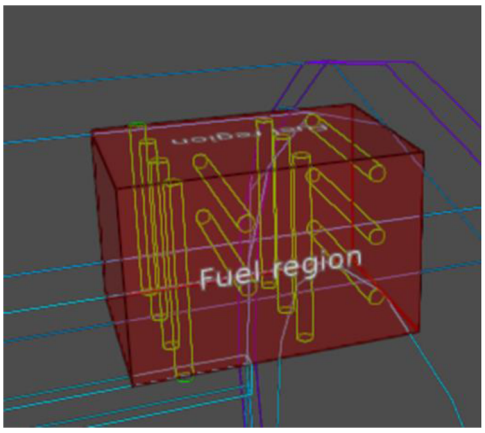


Fig. 10. The array of pipework congestion geometry used in the FLACS explosion simulations based on the geometry used in the HSE JIP Experiments [54].

Table 6
The initial conditions used in the FLACS explosion simulations for the quiescent and turbulent flammable gas cloud.

Parameter	Quiescent	Turbulent
Characteristic velocity (m/s)	0	200
Relative turbulence intensity	0	0.3
Turbulence length scale (m)	0	0.05

It was assumed that the explosion occurs whilst the aircraft is still stationary on the ground SLS (sea-level static) with an ambient temperature and pressure of 293 K and 100,325 Pa.

Two sizes of pressure relief vent were employed in the simulations. One was relatively small 0.2 m x 0.4 m (L x W), located at the top aft end of the compartment. This was intended to broadly correspond to the effective area (and operation) of the pressure relief doors used to manage burst air duct pressurisation hazards in a conventional nacelle compartment. The other was relatively large, 2.3 m x 0.9 m (L x W), running across the top of the compartment (this larger vent may also be considered to roughly correspond to the relief area conditions produced if a nacelle cowl door is forced open or even blown-off). In both cases a pressure panel (termed type "PLASTIC" in FLACS-CFD, that is intended to represent a simple panel type that will be removed from the simulation when the internal compartment pressure reaches a specified value [33] was introduced across the vent outlet and set to open when the internal pressure rise reached 0.0345 barg (0.5 psi). The pressure rise of 0.0345 barg (0.5 psi) was considered the lower limit of tolerable overpressure within the compartment. An upper tolerable limit of 0.1 barg (1.45 psi) was also assumed to represent the overpressure threshold at which significant structural damage to the compartment could occur (such a limit for major structural damage is typically used for buildings subjected to high explosives [53]). For simplicity a single threshold for structural damage, based on the maximum overpressure has been used in the analysis, but the explosion's rate of pressure rise, duration and impulse may also be important in determining the level of structural damage caused.

Two area-averaged pressure monitor panels were defined as strips running along the insides of the cowl at 90 degrees and 270 degrees. These were intended to correspond to the cowl door latches and provide an indication of the (area-averaged) pressure the latches are subjected to during an explosion.

For some simulations, an array of pipework congestion was introduced into the flammable gas cloud region Fig. 10. The pipework array geometry is based upon that employed in the HSE JIP test rig, which was used to determine the explosion overpressures for the ignition of methane-air clouds in a 2.5 m x 2.5 m x 14.9 m (94 m^3) enclosure [54]. The array consists of a staggered arrangement of pipes, each having a diameter of 25 mm, with a spacing of 3 pipe diameters between pipes, adjacent rows set at right angles and pipes staggered between every other row. To fit within the cowl compartment annulus, the 0.45 × 0.45 m x 0.45 m cloud volume used in the HSE JIP test rig was adjusted to occupy a volume of 0.45 m x 0.3 m x 0.3 m. The length of each pipe was reduced from 0.45 m to 0.3 m, and the total number of pipes used in the array was reduced from 16 to 12.

Initial conditions within the flammable gas cloud were set to be either quiescent or turbulent (Table 6) using the values recommended in the FLACS user guidelines [33]. In the case of the turbulent initial conditions, the recommended characteristic values are intended to represent the turbulence that would be generated by a high velocity gas jet release. FLACS user guidelines also suggest that the initial turbulence setting is likely to have little effect for ignition in highly congested regions, where turbulence will be quickly generated by the geometry. Hence, a quiescent initial condition was adopted for the simulations with a congested pipework geometry located in the flammable gas cloud region.

Several different locations for the flammable gas cloud region within the compartment were simulated to gauge sensitivity to this parameter. These were at the top of the compartment (forward, aft and centre) at the side (aft) and at the bottom of the compartment (forward and aft). In each case the position of the ignition source was also adjusted to match the location of the cloud.

A uniform grid cell size of was used inside the compartment region, where the flammable cloud is located. Outside the compartment, the grid cell size used between adjacent cells was expanded towards the boundaries by a factor of no more than 1.2. The annular compartment geometry was located with the central axis running along the x-axis and the origin located at the front centre of the compartment. The simulation domain used in the simulations extended from -2.5 m to 5.0 m in the x direction, -3.7 m to 3.7 m in the y direction and from -1.2 m to 8.7 m in the (vertical) z direction. This provided distances of 3 times the length of the compartment (2.5 m), in the direction of the explosion venting, to the top (+Z) boundary and the length of the compartment to the other boundaries located in the y and x directions. An initial grid sensitivity study was performed, using three different minimum grid cell sizes for the base case scenario (Run 1), as shown in Table 7. The results indicate that, when the grid cell size was reduced to 0.025 m, the deviation in the max overpressure for the baseline case was around 1% of that found using the smallest grid cell size. Although a greater level of grid sensitivity was found for the more complex scenarios, with high turbulence and pipework congestion, the predicted peak pressures remained within 10-20% of those found using the finest grid cell size. For a calibrated code, like FLACS-CFD, a degree of grid sensitivity is to be expected, and the results will not necessarily fully converge with increasing grid resolution [33]. In view of the other limitations and uncertainties associated with the analysis (see Section 5.7) a uniform grid cell size of 0.025 m inside the nacelle compartment was judged to produce acceptable results and was therefore used in the remaining explosion simulations.

Table 8 summarises the matrix of 16 FLACS-CFD explosion simulation runs that were undertaken.

Table 7
The grid sensitivity study results.

Min. grid cell size (m)	Total number of grid cells	Max pressure (barg)	Relative deviation
0.020	6,903,624	0.092	Ref.
0.025	3,862,820	0.093	1%
0.050	684,684	0.086	6%

Table 8
The matrix of FLACS-CFD simulation runs undertaken for the small H_2-air cloud nacelle compartment explosion scenario and the resulting peak maximum overpressure, peak area-averaged panel pressure and peak area-averaged panel impulse that were predicted for each run.

Run	Cloud Initial State	Vent size (m x m)	Congestion?	Cloud Location	Ignition Point (x, y, z) m	Pmax (barg)	Peak Panel Pressure (barg)	Peak Panel Impulse (Pa.s)
1	Quiescent	0.2 × 0.4	No	Fwd, Top	(0.0125, 0.0125, 0.8375)	0.096	0.062	206
2	Quiescent	2.3 × 0.9	No	Fwd, Top	(0.0125, 0.0125, 0.8375)	0.073	0.028	74
3	Quiescent	0.2 × 0.4	No	Aft, Top	(2.4875, 0.0125, 0.8375)	0.069	0.034	104
4	Quiescent	0.2 × 0.4	No	Centre, Top	(1.4375, 0.0125, 0.8375)	0.060	0.052	196
5	Quiescent	0.2 × 0.4	No	Aft, Side	(2.4875, 0.8375, 0.0125)	0.091	0.068	206
6	Quiescent	0.2 × 0.4	No	Aft, Bottom	(2.4875, 0.0125, -0.8375)	0.088	0.058	195
7	Quiescent	0.2 × 0.4	No	Fwd, Bottom	(0.0125, 0.0125, -0.8375)	0.091	0.059	194
8	Turbulent	0.2 × 0.4	No	Fwd, Top	(0.0125, 0.0125, 0.8375)	0.494	0.106	228
9	Turbulent	2.3 × 0.9	No	Fwd, Top	(0.0125, 0.0125, 0.8375)	0.266	0.051	63
10	Quiescent	0.2 × 0.4	Yes	Fwd, Top	(0.0125, 0.0125, 0.8375)	0.455	0.110	220
11	Quiescent	0.2 × 0.4	Yes	Aft, Top	(2.4875, 0.0125, 0.8375)	0.891	0.107	110
12	Quiescent	0.2 × 0.4	Yes	Fwd, Bottom	(0.0125, 0.0125, -0.8375)	0.470	0.112	251
13	Quiescent	2.3 × 0.9	Yes	Fwd, Top	(0.0125, 0.0125, 0.8375)	0.409	0.057	28
14	Quiescent	2.3 × 0.9	Yes	Aft, Top	(2.4875, 0.0125, 0.8375)	0.444	0.059	28
15	Quiescent	0.2 × 0.4	Yes	Centre, Top	(1.4375, 0.0125, 0.8375)	0.325	0.098	87
16	Quiescent	2.3 × 0.9	Yes	Centre, Top	(1.4375, 0.0125, 0.8375)	0.132	0.045	33

4.2. Results

The results indicate that both the initial turbulence level of the flammable cloud and the introduction of pipework congestion into the cloud have a significant effect on the explosion overpressure behaviour. Fig. 11 (a-b) compares the effect of using turbulent (run 8) and quiescent (run 1) initial conditions on the resulting overpressure-time histories. The turbulent initial cloud generates a higher flame propagation rate and much higher local peak overpressures, particularly in the confined region where the cloud is adjacent to forward bulkhead wall. High initial turbulence also increases the peak area average panel pressure exerted along the side walls of compartment. The magnitude of the maximum explosion overpressure and the area-averaged panel pressure are significantly increased, relative to those predicted under quiescent conditions. Both pressure peaks exceed the 0.1 barg threshold and also occur at a much shorter time interval after ignition. Fig. 11 (c-d) show a comparison between the overpressure-time histories obtained for the flammable gas cloud with (run 10) and without (run 1) the array of pipework congestion present. Introducing congestion into the cloud results in the generation of turbulence, significantly increasing the rate

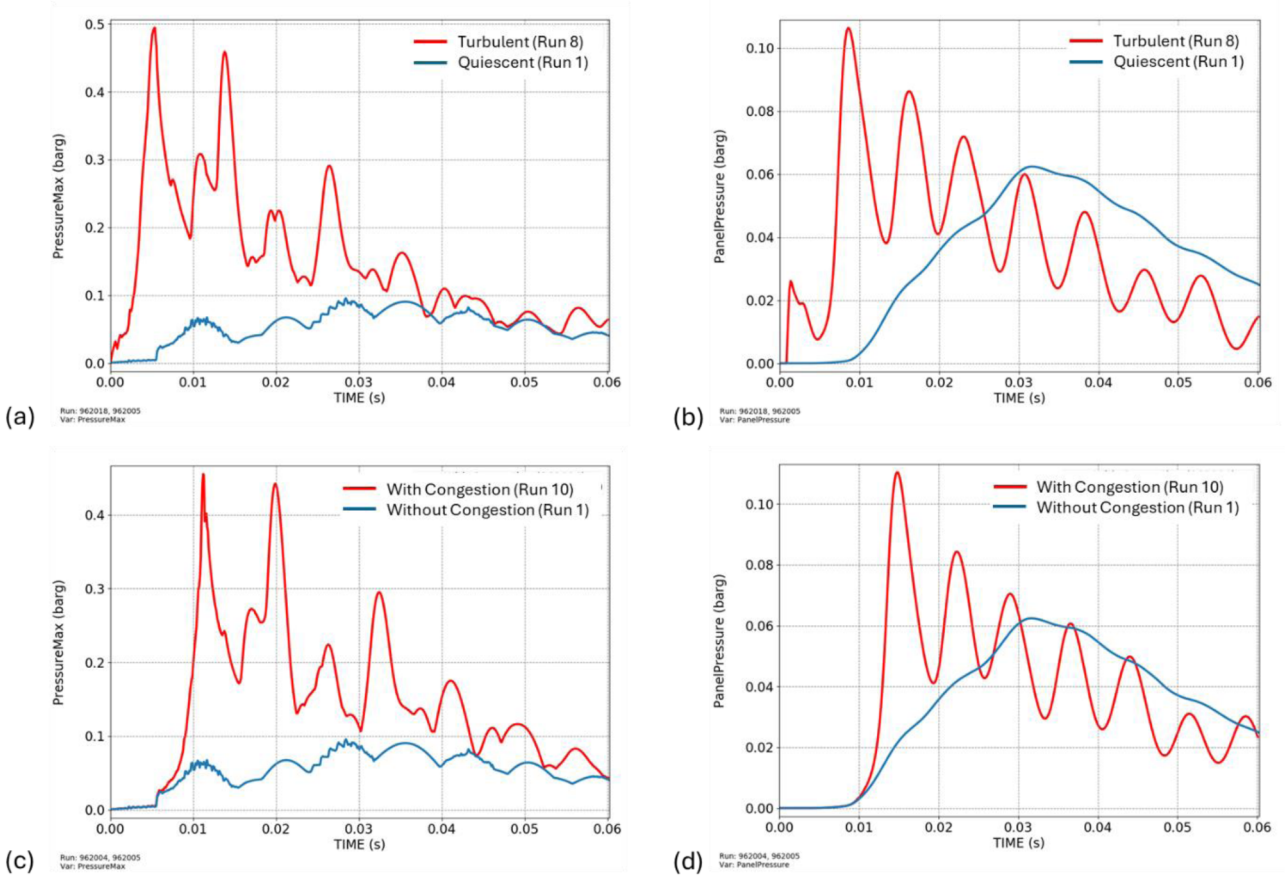


Fig. 11. The effect of: (a-b) turbulent versus quiescent initial conditions for the flammable cloud; and (c-d) cloud with and without an array of pipework congestion on the simulated maximum overpressure and area-averaged panel overpressure versus time.

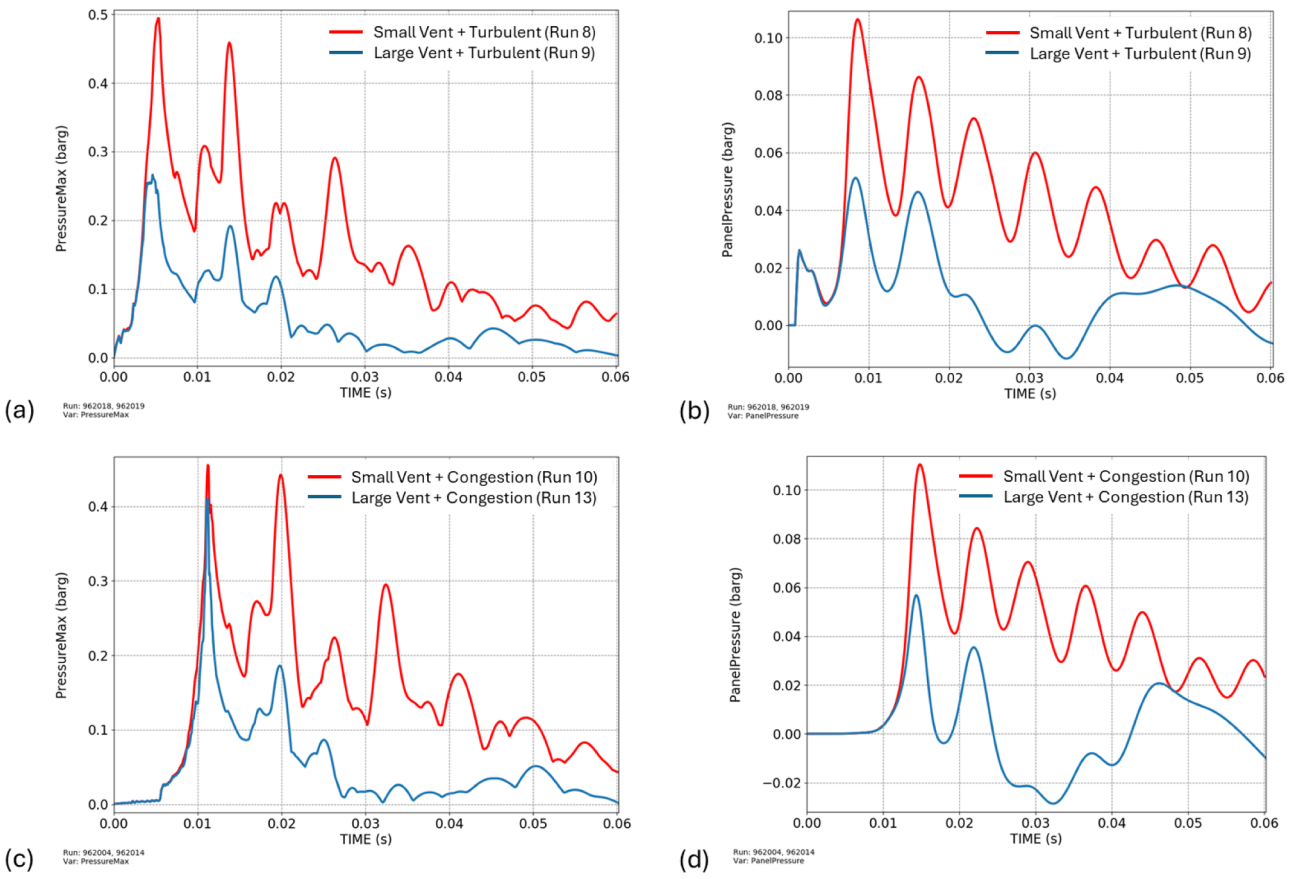


Fig. 12. The effect of using a large versus a small pressure relief vent area on the explosion behaviour of: (a-b) a flammable cloud with a high level of initial turbulence; and (c-d) a flammable cloud with an array of pipework congestion present, on the simulated maximum overpressure and area-averaged panel overpressure versus time.

of flame propagation and size of the peak overpressures produced relative to the uncongested case. Both the maximum overpressure and area-averaged panel pressure exceed the 0.1 barg threshold.

The results suggest that the size of the pressure relief panel used also has a significant effect on the explosion behaviour. Fig. 12 (a-b) compares the effect of using a small or large area vent panel on the resulting pressure-time history predicted with a turbulent initial condition. The larger vent area reduces the magnitude of the peak overpressure produced by the turbulent cloud, but high local overpressures, exceeding the 0.1 threshold, are still generated in the region where the cloud is adjacent to the bulkhead wall. The area-averaged panel pressure predicted for the large vent area case is also significantly lower, with the peak falling well below the 0.1 threshold. Increasing the size of the vent panel used also has a similar effect on the cases with the array of pipework congestion, as shown in Fig. 12 (c-d). With the large area vent present both the maximum overpressure and area-averaged panel pressure are significantly reduced.

The peak (global) maximum pressure and peak area-averaged panel pressure results found for each run are summarised in Table 8. Examination of these results suggests that the peak overpressures remain at a tolerable level (< 0.1 barg) for the cases with quiescent initial conditions and do not appear to be very sensitive to the location of the cloud within the compartment. The results also show that the peak overpressure and panel pressure exceeds the 0.1 barg tolerable threshold for the cases with turbulent initial conditions or pipework congestion located in the flammable cloud, unless a large relief vent is fitted. In such cases the peak area-averaged panel overpressure is predicted to be reduced to tolerable levels, although the peak maximum (point) pressure still exceeds the upper threshold. The table also summarises the peak area-averaged panel impulse that is predicted for each of the runs. The peak panel impulse is significantly lower for those cases where a large pressure vent is used. For the cases with a smaller vent, the peak panel impulse is also lower when the flammable cloud is located directly below the vent opening (aft, top). The results also suggest that the magnitude of the peak panel impulse produced is relatively insensitive to the introduction of turbulent initial conditions or pipework congestion.

5. Discussion

A hybrid modelling strategy, using two different codes was employed as a means of exploiting the strengths of each - STAR CCM+ for higher fidelity dispersion modelling of hydrogen leaks in the nacelle compartment and FLACS-CFD as an explosion focused solver which has been extensively validated for application to hydrogen explosion simulations. The CFD dispersion model was used to examine the formation and behaviour of flammable hydrogen clouds in the nacelle compartment. The dispersion modelling results were also used to assess the size of equivalent stoichiometric hydrogen-air cloud that would be formed in the compartment for a given hydrogen leak rate (Table 5). Hence, the size of the equivalent stoichiometric H_2-air cloud used in the FLACS explosion simulations can be related to a hydrogen leak rate of around 0.1 g/s. Although it may have been technically possible to map the gas concentrations obtained from the dispersion simulations directly into the explosion simulations, using an equivalent stoichiometric flammable gas cloud with the FLACS explosion model is a standard approach that has been used in a number of safety studies (e.g. Vye and Mills [31]). Using an equivalent stoichiometric gas cloud is also the recommended

assessment method specified in the international safety standard for stationary gas turbine enclosures ISO 21789 [55]. Hence a similar approach was adopted here.

The simulation results obtained here suggest that a stoichiometric hydrogen-air cloud occupying 1% of the nacelle compartment volume, and containing 1 g of hydrogen, could be capable of producing explosion overpressure exceeding a tolerable overpressure limit of 0.1 barg (under turbulent or congested conditions, unless a large pressure relief vent is used). Hence the results suggest that (for a relief vent area of 0.2 m x 0.4 m, 0.08 m^2) an upper limit of acceptable leak size would be less than 1% of compartment volume (and less than 1 g of hydrogen).

Is the suggested explosion challenge posed by such relatively small amounts of hydrogen in the nacelle compartment plausible? A comparison can be made with ISO 21789 [55], which sets out the compliance requirements for a flammable gas leak within a fixed gas turbine enclosure for methane fuels. In the standard, 10 mbarg is adopted as a limiting explosion overpressure rise for the turbine enclosure to avoid significant damage. To limit explosion overpressure in the enclosure to less than 10 mbarg sufficient ventilation of the enclosure is required such that the stoichiometric volume of the equivalent flammable gas cloud formed by a leak occupies less than 0.1% of the enclosure volume. The basis for this 0.1% enclosure volume criteria is experimental test work carried out HSE JIP to determine explosion overpressures for the ignition of methane-air clouds in a 2.5 m x 2.5 m x 14.9 m (94 m^3) enclosure [54]. Hence, to maintain the explosion overpressure threshold below a 10 mbarg threshold, the equivalent stoichiometric cloud is required to be less than 0.1% of the compartment volume – even for a significantly larger gas turbine enclosure volume using methane gas as a fuel.

Vye and Miles [31] used FLACS-CFD to model the HSE JIP experimental test rig and extend the analysis to hydrogen. Their results suggest that to keep the explosion overpressure < 10 mbarg in a gas turbine enclosure the stoichiometric volume of the equivalent flammable gas cloud would need to be $< 0.022\%$ of the enclosure volume – because hydrogen is a more reactive gas. For a smaller nacelle cowl compartment volume of 4 m^3 applying this criterion would require limiting any hydrogen leaks to a very small equivalent stoichiometric flammable cloud leak volume of 0.00088 m^3 (or leak mass around 0.02 g) which could be hard to achieve.

Thus, comparison with the criteria used for fixed gas turbine enclosures would suggest that the results obtained here are plausible, and that the explosion overpressure generated by even a relatively small hydrogen leak volume into a nacelle cowl compartment could be challenging to manage to a tolerable level using air-based ventilation.

5.1. Model validation

There is currently a lack of suitable experimental test data for hydrogen hazards in annular compartment type geometries and operating conditions with which to test and validate the performance of model predictions. To have the necessary level of confidence in the models suitable experimental test data will be required to validate the modelling tools. This work will allow the consequences of leaks and physical processes in aircraft engine compartments to be determined more accurately and the data generated will be used to assess model limitations and uncertainties and improve their predictive capabilities.

5.2. The impact of an explosion on internal pipework within the nacelle

An explosion shock wave in a nacelle compartment can impose very high, short-duration pressures and drag forces on internal pipework, causing vibration, bending, support failure, and in severe cases permanent deformation, buckling, or rupture, triggering the occurrence of hazardous secondary leaks. The confined nature of a compartment makes this worse since reflections from walls and equipment can amplify and prolong the load.

5.3. Simplified nacelle geometry and lack of internal obstacles

Although it wasn't explicitly considered in the dispersion simulations, it seems likely that the introduction of internal congestion into the compartment would strongly affect hydrogen dispersion behaviour and inhibit the effectiveness of air ventilation. This would serve to further concentrate the flammable cloud, reducing the acceptable/tolerable hydrogen leak rate below that found for an empty nacelle compartment (< 0.1 g/s). Furthermore, since the explosion simulations clearly show that presence of congestion will significantly increase flame acceleration behaviour and peak explosion overpressures the results suggest that hydrogen leaks into regions of the nacelle compartment containing internal congestion should be avoided.

5.4. LH_2 hydrogen hazards

The analysis presented here has concentrated primarily on the hazards due to gaseous hydrogen releases into the nacelle. Liquid or cryogenic hydrogen releases (below 100 K) into the compartment will pose additional hazards due to both the direct effects of very cold temperatures on materials and the nacelle structure and phase change effects due to vapourisation of liquid hydrogen and freezing of the air.

5.5. Hydrogen dispersion and venting behaviour under flight conditions

The modelling analysis presented here has looked mainly at examining hydrogen dispersion and explosion behaviour for an engine nacelle compartment operating on the ground, under sea-level static (SLS) conditions. The effect of altitude pressure and temperature conditions on hydrogen explosion behaviour now needs to be further generalised to consider the effect of flight operating conditions on hydrogen dispersion behaviour, including different nacelle compartment orientations and the impact of high velocity external airflows and their effect upon hydrogen ventilation behaviour. A suitable research framework would examine how high-altitude conditions (low ambient pressure, low temperature, and high external airspeed) modify hydrogen leak dispersion, and explosion behaviour for the nacelle compartment. Low pressure and temperature conditions will modify hydrogen-air flammability limits, flame speeds and explosion overpressures, while high airspeed drives nacelle ventilation that can either disperse or redistribute leaked hydrogen in the compartment. The framework should combine altitude-dependent leak modelling of hydrogen dispersion in the confined nacelle geometry and explosion simulations of the resulting flammable clouds to assess flame acceleration, overpressure, and structural loads. Experimental validation using reduced-pressure chambers and explosion tests would support model development. The results would inform nacelle design, ventilation requirements and safety measures for hydrogen-powered aircraft.

5.6. The safety margin in the recommended tolerable hydrogen leak rate threshold

The total mass of hydrogen (1.27 g) used to determine the size of the equivalent stoichiometric cloud for the 0.1 g/s leak case, is highly conservative. The simulation results indicate that that actual mass of hydrogen falling in the flammable range for the 0.1 g/s leak case is at least an order of magnitude lower than this. Hence there is a significant safety margin - of a factor of 10 - in the recommended tolerable leakage rate threshold of 0.1 g/s. This should compensate for the effect of other uncertainties due to the impact of dynamic factors such as vibration and airflow disturbance.

5.7. Modelling limitations and uncertainties

There is at present significant uncertainty surrounding the modelling of hydrogen accident scenarios in nacelle compartment geometries and

operating conditions, due to the lack of suitable experimental test data with which to validate the models with. The modelling predictions made in this study must therefore be treated with a degree of caution given these difficulties over validation. When considering the results of the modelling analysis performed here the following limitations and uncertainties should be borne in mind:

- A limitation in the turbulence model used in FLACS-CFD also effectively imposes a lower bound on the grid size that should be used in explosion simulations. For grid cells of around 1 cm or less, artificial turbulence is generated in the cell, due to limitations in how the turbulence model deals with boundary layer effects at these scales (note that the limitation is generally regarded as being conservative, since it will cause overpressures to be over-predicted) [33].
- The dispersion results were obtained for an empty nacelle compartment without internal pipework or other congestion. The introduction of internal congestion into the compartment would likely inhibit hydrogen dispersion behaviour and the effectiveness of air ventilation, potentially further increasing the local hydrogen concentration and associated explosion overpressure.
- Blind explosion simulations performed using FLACS-CFD (with characteristics conforming to previous validated cases) typically have associated uncertainties in the range of ±30-40% when compared against experiment [33]. However, for unvalidated cases (such as the nacelle compartment geometry) the uncertainty in the predicted overpressures may be significantly higher (by a factor of 2 or more) [56].
- Star CCM+ has not previously received the same level of validation against experimental test data for hydrogen as has FLACS-CFD. Initial validation studies comparing the predictions of Star-CCM+ were found to be in good agreement with the experimental data, but further validation work is required to more fully establish the uncertainties and limitations in the code's predictions for hydrogen dispersion behaviour.

6. Conclusion

This study presents the first detailed CFD-based analysis of hydrogen leak dispersion and explosion hazards within an aircraft engine nacelle compartment, addressing a critical gap in aviation safety knowledge. By combining STAR-CCM+ and FLACS-CFD simulations, the research quantifies the formation of flammable hydrogen clouds and resulting explosion overpressures under various leak and ventilation scenarios.

The key quantitative results of the nacelle compartment hydrogen leak dispersion study suggest that:

- Significant flammable hydrogen cloud volumes and masses could form within the nacelle compartment for hydrogen leak rates > 0.1 g/s
- The form and extent of the flammable cloud formed in the nacelle compartment is influenced by the mass flow rate, location and orientation of the hydrogen leak – relative to the airflow direction, as well as the ventilation rate and proximity of the vent to the leak source. The mass of hydrogen can be reduced by a factor of up to 8 times if it is located in close proximity to and orientated towards the vent.
- Hydrogen leak rates up to around 2 g/s tend to produce localised flammable hydrogen clouds and stratified layers at the top of the compartment rather than being uniformly mixed throughout the compartment
- The steady-state mass of hydrogen accumulating in the upper part of the compartment predicted for the case of 1 g/s with 5 ACM is ~ 8.5 kg. A smaller hydrogen leak rate of 0.1 g/s produced only a localised plume around the leak source and a total hydrogen mass in the compartment ~ 1 g. Conversely a steady-state hydrogen leak of 5 g/s is predicted to completely fill the compartment with hydrogen with a mass ~ 26 g. A lower flammable mass is predicted in the compartment for leak scenarios where the leak is both located close to and directed towards the vent outlet.

The key quantitative results of the nacelle compartment explosion modelling study suggest that:

- Under quiescent conditions the peak explosion overpressures are predicted to remain at tolerable levels (< 0.1 barg) and appear to be relatively insensitive to the location of the cloud in the cowl compartment.
- Both the maximum and peak area-averaged panel explosion overpressures generated by ignition of the cloud are increased significantly by a factor of 2 to 4 times by introducing:
  - high levels of initial turbulence (as would be induced by a large jet hydrogen leak)
  - pipework congestion into the hydrogen gas cloud region
- Hydrogen leaks into regions of the nacelle compartment containing internal pipework or congestion should be avoided
- The peak area-averaged panel overpressures along the sides of the compartment are predicted to exceed tolerable level (> 0.1 barg), under turbulent and congested cloud conditions, unless a large pressure relief vent area is used.
- The peak area-averaged panel impulse levels appear to be more sensitive to pressure relief vent area and (to a lesser extent) the proximity of the cloud to the vent, than initial turbulence or congested cloud conditions. The use of a large vent can reduce the magnitude of the peak impulse by a factor of 4 to 8 times.
- Using a large pressure relief vent area significantly reduces the maximum overpressure – but high local peak pressures are still predicted in regions where the cloud is adjacent to the compartment walls.
- In order to maintain the peak area-averaged explosion overpressures generated in a nacelle compartment (with a 0.08 m2 vent area) to tolerable levels (< 0.1 barg), the volume of the equivalent stoichiometric hydrogen-air cloud formed by a hydrogen leak, under turbulent or congested conditions, would need to be maintained well below 1% of the compartment volume.

The analysis suggest that air-based ventilation alone may be insufficient to safely manage the explosion hazard posed by larger hydrogen leaks (> 0.1 g/s) into an aircraft engine nacelle compartment and that alternative mitigation measures could be required to provide resilience.

Based upon the results of the analysis the following hydrogen hazard prevention and mitigation measures are recommended to protect the nacelle compartment:

i) Preventing hydrogen leaks by using double walled piping or some other form of secondary enclosure around valves, flanges and seals;
ii) Rapid hydrogen leak detection and emergency system shutdown;
iii) Nitrogen gas injection into the compartment to produce an inerted atmosphere maintaining the oxygen concentration below the 5% (v/v) limiting oxygen concentration (LOC) required for combustion in H2-O2-N2 atmospheres;
iv) Using a large area blowout panel (or series of smaller pressure relief doors of equivalent area) located at the top of the H2 compartment that would open to relieve the explosion overpressure in the event that a flammable mixture was to form and be ignited.

The novelty of this research is that it is the first study to systematically model and quantify hydrogen leak and explosion hazards specifically within an aircraft engine nacelle compartment, addressing a critical gap

in aviation safety knowledge. It also explores the interaction between leak characteristics, ventilation, and compartment geometry - a previously unaddressed area in hydrogen aviation safety.

The contribution of this study is that it provides quantitative thresholds for flammable hydrogen cloud formation and explosion overpressure in nacelle compartments. It demonstrates that even small hydrogen leaks (> 0.1 g/s) can form flammable clouds capable of producing hazardous explosion overpressures, especially under turbulent or congested conditions. It also shows that air-based ventilation alone may be insufficient to mitigate explosion hazards from hydrogen leaks and offers design guidance on acceptable leak rates, ventilation requirements, and pressure relief vent sizing.

The potential impact of this study is that it supports the certification and safety assessment of hydrogen-fuelled aircraft engine powerplants. It informs the regulatory development and industry standards for hydrogen leak management in aviation. It also enhances the understanding of explosion dynamics in confined aircraft compartments, which is vital for risk mitigation and aircraft safety.

CRediT authorship contribution statement

Paul Holborn: Writing – original draft, Visualization, Methodology, Investigation, Formal analysis, Conceptualization. **Xiaoxiao Sun:** Writing – review & editing, Visualization, Methodology, Investigation, Formal analysis. **Vishal Sethi:** Writing – review & editing, Supervision. **Michael Willmot:** Writing – review & editing, Supervision.

Declaration of competing interest

The authors declare that they have no known competing financial interests or personal relationships that could have appeared to influence the work reported in this paper.

Acknowledgements

The authors thank Rolls-Royce plc for funding this work as part of the ATI project RACHEL, Project Ref: 10039810. Due to commercial confidentiality agreements the supporting data is not available.

Data availability

The data that has been used is confidential.

References

[1] McKinsey & Company, Hydrogen-powered Aviation: a fact-based study of hydrogen technology, economics, and climate impact by 2050. https://www.h2knowledgecentre.com/content/researchpaper3981, 2020 accessed January 9, 2026.
[2] C. Hughes, C. Gear, Our vision for zero-carbon emission air travel. https://www.ati.org.uk/wp-content/uploads/2022/03/FZO-ALL-REP-0004-FlyZero-Our-Vision-for-Zero-Carbon-Emission-Air-Travel.pdf, 2022 accessed January 6, 2025.
[3] Clean Aviation Joint Undertaking, Strategic research and innovation agenda—towards disruptive technologies for new generation aircraft by 2035. https://clean-aviation.eu/sites/default/files/2024-09/2024-Clean-Aviation-SRIA.pdf, 2024 (accessed January 6, 2026).
[4] G.D. Brewer, Hydrogen Aircraft Technology, CRC Press, Boca Raton, 1991.
[5] A. Contreras, S. Yiğit, K. Özay, T.N. Veziroğlu, Hydrogen as aviation fuel: a comparison with hydrocarbon fuels, Int. J. Hydrogen Energy 22 (1997) 1053–1060, https://doi.org/10.1016/S0360-3199(97)00008-6.
[6] H.W. Pohl, V.V. Malychev, Hydrogen in future civil aviation, Int. J. Hydrogen Energy 22 (1997) 1061–1069, https://doi.org/10.1016/S0360-3199(95)00140-9.
[7] H. Nojoumi, I. Dincer, G.F. Naterer, Greenhouse gas emissions assessment of hydrogen and kerosene-fueled aircraft propulsion, Int. J. Hydrogen Energy 34 (2009) 1363–1369, https://doi.org/10.1016/j.ijhydene.2008.11.017.
[8] B. Khandelwal, A. Karakurt, P.R. Sekaran, V. Sethi, R. Singh, Hydrogen powered aircraft : the future of air transport, Prog. Aerosp. Sci. 60 (2013) 45–59, https://doi.org/10.1016/j.paerosci.2012.12.002.
[9] D. Verstraete, Long range transport aircraft using hydrogen fuel, Int. J. Hydrogen Energy 38 (2013) 14824–14831, https://doi.org/10.1016/j.ijhydene.2013.09.021.
[10] D. Verstraete, On the energy efficiency of hydrogen-fuelled transport aircraft, Int. J. Hydrogen Energy 40 (2015) 7388–7394, https://doi.org/10.1016/j.ijhydene.2015.04.055.
[11] M. Prewitz, A. Bardenhagen, R. Beck, Hydrogen as the fuel of the future in aircrafts – Challenges and opportunities, Int. J. Hydrogen Energy 45 (2020) 25378–25385, https://doi.org/10.1016/j.ijhydene.2020.06.238.
[12] R.V.V. Petrescu, A. Machín, K. Fontánez, J.C. Arango, F.M. Márquez, F.I. T. Petrescu, Hydrogen for aircraft power and propulsion, Int. J. Hydrogen Energy 45 (2020) 20740–20764, https://doi.org/10.1016/j.ijhydene.2020.05.253.
[13] C. Mourouzidis, G. Singh, X. Sun, J. Huete, D. Nalianda, T. Nikolaidis, V. Sethi, A. Rolt, E. Goodger, P. Pilidis, Abating CO2 and non-CO2 emissions with hydrogen propulsion, Aeronaut. J. 128 (2024) 1576–1593, https://doi.org/10.1017/aer.2024.20.
[14] V. Sethi, X. Sun, D. Nalianda, A. Rolt, P. Holborn, C. Wijesinghe, C. Xisto, I. Jonsson, T. Grönstedt, J. Ingram, A. Lundbladh, A. Isikveren, I. Williamson, T. Harrison, A. Yenokyan, Enabling cryogenic hydrogen-based CO2-free air transport: meeting the demands of zero carbon aviation, IEEE Electr. Mag. 10 (2022) 69–81, https://doi.org/10.1109/MELE.2022.3165955.
[15] E.J. Adler, J.R.R.A. Martins, Hydrogen-powered aircraft: Fundamental concepts, key technologies, and environmental impacts, Prog. Aerosp. Sci. 141 (2023) 100922, https://doi.org/10.1016/j.paerosci.2023.100922.
[16] S. Tiwari, M.J. Pekris, J.J. Doherty, A review of liquid hydrogen aircraft and propulsion technologies, Int. J. Hydrogen Energy 57 (2024) 1174–1196, https://doi.org/10.1016/j.ijhydene.2023.12.263.
[17] A. Ebrahimi, A. Rolt, S. Jafari, J.H. Anton, A review on liquid hydrogen fuel systems in aircraft applications for gas turbine engines, Int. J. Hydrogen Energy 91 (2024) 88–105, https://doi.org/10.1016/j.ijhydene.2024.10.121.
[18] R. Spencer, Certification considerations for the configuration of a hydrogen-fuelled aeroplane, Aeronaut. J. 127 (2023) 213–231, https://doi.org/10.1017/aer.2022.79.
[19] EASA Certification Roadmap on H2 — International Workshop 2024. https://www.easa.europa.eu/en/newsroom-and-events/events/easa-certification-roadmap-h2-international-workshop-2024, 2024 accessed January 6, 2026.
[20] FAA, Hydrogen-Fueled Aircraft Safety and Certification Roadmap, Federal Aviation Administration, 2024.
[21] F. Rigas, P. Amyotte, Hydrogen Safety: Production, Transport, Storage, Use, and the Environment, 1st ed., CRC Press, Boca Raton, 2012 https://doi.org/10.1201/9781003313007.
[22] A. Kotchourko, T. Jordan, Hydrogen Safety for Energy Applications: Engineering Design, Risk Assessment, and Codes and Standards, Butterworth-Heinemann, 2022.
[23] C.M. Benson, P.G. Holborn, A.M. Rolt, J.M. Ingram, E. Alexander, Combined Hazard Analyses to Explore the Impact of Liquid Hydrogen Fuel on the Civil Aviation Industry, American Society of Mechanical Engineers Digital Collection, 2021, https://doi.org/10.1115/GT2020-14977.
[24] J.M. Ingram, C.M. Benson, P.N. Battersby, D4.2a: Test report on hydrogen flammability and ignition under altitude conditions, n.d. https://cordis.europa.eu/project/id/769241/results, 2026. accessed January 6
[25] P.G. Holborn, J.M. Ingram, C. Benson, Modelling studies of the hazards posed by liquid hydrogen use in civil aviation, IOP Conf. Ser.: Mater. Sci. Eng. 1226 (2022) 012059, https://doi.org/10.1088/1757-899X/1226/1/012059.
[26] FAA, Energy supply device aviation rulemaking committee, 2019.
[27] HEAVEN, HEAVEN cryogenic hydrogen tech aircraft. https://heaven-fch-project.eu/, 2023 accessed January 6, 2026.
[28] J. Jézégou, A.M. Almeida-Marino, G. O'sullivan, B.J. Carrasco, R. André, Y. Gourinat, Certification gap analysis for normal-category and large hydrogen-powered airplanes, Aerospace 12 (2025) 239, https://doi.org/10.3390/aerospace12030239.
[29] EASA, Certification specifications and acceptable means of compliance for large aeroplanes (CS-25). https://www.easa.europa.eu/en/document-library/easy-access-rules/online-publications/easy-access-rules-large-aeroplanes-cs-25?page=1, 2023 accessed January 6, 2026.
[30] CAA, UK CAA Hydrogen Challenge CS-25 Gap Analysis for a Hydrogen Fuel System, UK Civil Aviation Authority, UK, 2025. https://www.caa.co.uk/data-and-publications/publications/documents/content/cap3124/.
[31] T.S. Vye, D. Miles, Gas Turbine Enclosures: Determining Ventilation Safety Criteria using Hydrogen Explosion Modelling, in: 9th International Conference on Hydrogen Safety ICHS, 2021.
[32] Siemens, Simcenter Star-CCM+ 2310 User Guide, 2023.
[33] Gexcon, FLACS-CFD v22.2 user's manual, (2023).
[34] V. Molkov, Fundamentals of hydrogen safety engineering I and II, Bookboon.Com (2012).
[35] B.D. Ehrhart, E.S. Hecht, B.B. Schroeder, K.M. Groth, J.T. Reynolds, M.L. Blaylock, E.E. Carrier, Hydrogen Plus Other Alternative Fuels Risk Assessment Models (HyRAM+) Version 5.1 Technical Reference Manual, Sandia National Laboratories (SNL-NM), Albuquerque, NM (United States), 2023, https://doi.org/10.2172/2369637.
[36] B.C.R. Ewan, K. Moodie, Structure and Velocity Measurements in Underexpanded Jets, Combust. Sci. Technol. 45 (1986) 275–288, https://doi.org/10.1080/00102208608923857.
[37] A. Velikorodny, S. Kudriakov, Numerical study of the near-field of highly underexpanded turbulent gas jets, Int. J. Hydrogen Energy 37 (2012) 17390–17399, https://doi.org/10.1016/j.ijhydene.2012.05.142.
[38] S. Patankar, Numerical Heat Transfer and Fluid Flow, CRC Press, Boca Raton, 1980, https://doi.org/10.1201/9781482234213.
[39] R.G. Abdel-Gayed, D. Bradley, M. Lawes, Turbulent burning velocities: a general correlation in terms of straining rates, Proceed. Royal Soc. London. A. Mathe. Phys. Sci. 414 (1987) 389–413, https://doi.org/10.1098/rspa.1987.0150.
[40] N.R. Popat, C.A. Catlin, B.J. Arntzen, R.P. Lindstedt, B.H. Hjertager, T. Solberg, O. Saeter, A.C. Van den Berg, Investigations to improve and assess the accuracy of

computational fluid dynamic based explosion models, J. Hazard. Mater. 45 (1996) 1–25, https://doi.org/10.1016/0304-3894(95)00042-9.
[41] O. Hansen, J. Renoult, M. Sherman, S. Tiezen, Validation of FLACS-HYDROGEN CFD consequence prediction model against large scale H2 explosion experiments in the FLAME facility, in: Pisa, Italy, 2005.
[42] P. Middha, O.R. Hansen, I.E. Storvik, Validation of CFD-model for hydrogen dispersion, J. Loss Prev. Proc. Ind. 22 (2009) 1034–1038, https://doi.org/10.1016/j.jlp.2009.07.020.
[43] P. Middha, O.R. Hansen, Using computational fluid dynamics as a tool for hydrogen safety studies, J. Loss Prev. Proc. Ind. 22 (2009) 295–302, https://doi.org/10.1016/j.jlp.2008.10.006.
[44] E. Gallego, E. Migoya, J.M. Martín-Valdepeñas, A. Crespo, J. García, A. Venetsanos, E. Papanikolaou, S. Kumar, E. Studer, Y. Dagba, T. Jordan, W. Jahn, S. Høiset, D. Makarov, J. Piechna, An intercomparison exercise on the capabilities of CFD models to predict distribution and mixing of H2 in a closed vessel, Int. J. Hydrogen Energy 32 (2007) 2235–2245, https://doi.org/10.1016/j.ijhydene.2007.04.009.
[45] A.G. Venetsanos, E. Papanikolaou, M. Delichatsios, J. Garcia, O.R. Hansen, M. Heitsch, A. Huser, W. Jahn, T. Jordan, J.-M. Lacome, H.S. Ledin, D. Makarov, P. Middha, E. Studer, A.V. Tchouvelev, A. Teodorczyk, F. Verbecke, M.M. Van der Voort, An inter-comparison exercise on the capabilities of CFD models to predict the short and long term distribution and mixing of hydrogen in a garage, Int. J. Hydrogen Energy 34 (2009) 5912–5923, https://doi.org/10.1016/j.ijhydene.2009.01.055.
[46] A.G. Venetsanos, E. Papanikolaou, O.R. Hansen, P. Middha, J. Garcia, M. Heitsch, D. Baraldi, P. Adams, HySafe standard benchmark Problem SBEP-V11: predictions of hydrogen release and dispersion from a CGH2 bus in an underpass, Int. J. Hydrogen Energy 35 (2010) 3857–3867, https://doi.org/10.1016/j.ijhydene.2010.01.034.
[47] D. Makarov, F. Verbecke, V. Molkov, O. Roe, M. Skotenne, A. Kotchourko, A. Lelyakin, J. Yanez, O. Hansen, P. Middha, S. Ledin, D. Baraldi, M. Heitsch, A. Efimenko, A. Gavrikov, An inter-comparison exercise on CFD model capabilities to predict a hydrogen explosion in a simulated vehicle refuelling environment, Int. J. Hydrogen Energy 34 (2009) 2800–2814, https://doi.org/10.1016/j.ijhydene.2008.12.067.
[48] E. Vyazmina, S. Jallais, Validation and recommendations for FLACS CFD and engineering approaches to model hydrogen vented explosions: Effects of concentration, obstruction vent area and ignition position, Int. J. Hydrogen Energy 41 (2016) 15101–15109, https://doi.org/10.1016/j.ijhydene.2016.05.189.
[49] I.C. Tolias, J.R. Stewart, A. Newton, J. Keenan, D. Makarov, J.R. Hoyes, V. Molkov, A.G. Venetsanos, Numerical simulations of vented hydrogen deflagration in a medium-scale enclosure, J. Loss Prev. Proc. Ind. 52 (2018) 125–139, https://doi.org/10.1016/j.jlp.2017.10.014.
[50] T. Skjold, H. Hisken, S. Lakshmipathy, G. Atanga, M. Carcassi, M. Schiavetti, J. R. Stewart, A. Newton, J.R. Hoyes, I.C. Tolias, A.G. Venetsanos, O.R. Hansen, J. Geng, A. Huser, S. Helland, R. Jambut, K. Ren, A. Kotchourko, T. Jordan, J. Daubech, G. Lecocq, A.G. Hanssen, C. Kumar, L. Krumenacker, S. Jallais, D. Miller, C.R. Bauwens, Blind-prediction: Estimating the consequences of vented hydrogen deflagrations for homogeneous mixtures in 20-foot ISO containers, Int. J. Hydrogen Energy 44 (2019) 8997–9008, https://doi.org/10.1016/j.ijhydene.2018.06.191.
[51] T. Skjold, H. Hisken, S. Lakshmipathy, G. Atanga, L. Bernard, M. van Wingerden, K. L. Olsen, M.N. Holme, N.M. Turøy, M. Mykleby, K. van Wingerden, Vented hydrogen deflagrations in containers: Effect of congestion for homogeneous and inhomogeneous mixtures, Int. J. Hydrogen Energy 44 (2019) 8819–8832, https://doi.org/10.1016/j.ijhydene.2018.10.010.
[52] P. Roberts, L.C. Shirvill, T.A. Roberts, C.J. Butler, M. Royle, Dispersion of hydrogen from high pressure sources, Hazard XIX, Proc. Saf. Environ. Prot. (2006).
[53] D. Bjerketvedt, J.R. Bakke, K. van Wingerden, Gas explosion handbook, J. Hazard. Mater. 52 (1997) 1–150, https://doi.org/10.1016/S0304-3894(97)81620-2.
[54] D. Pritchard, Outstanding safety questions concerning the use of gas turbines for power generation – Final report on the experimental programme of work, Health and Safety Laboratory, Buxton, 2003.
[55] BS EN ISO 21789:2022 Gas turbine applications - Safety, (2022). https://doi.org/10.3403/30371933.
[56] C.J. Lea, H.S. Ledin, A review of the state-of-the-art in gas explosion modelling, Health and Safety Laboratory, 2002.



https://dspace.org/

An analysis of engine nacelle compartment leak and explosion hazards for a hydrogen-fuelled aircraft

Holborn, Paul; Sun, Xiaoxiao; Sethi, Vishal; Willmot, Michael

2026-10
Elsevier
https://doi.org/10.1016/j.ast.2026.112913
Holborn P, Sun X, Sethi V, Willmot M. (2026) An analysis of engine nacelle compartment leak and explosion hazards for a hydrogen-fuelled aircraft. Aerospace Science and Technology, Volume 177, Part D, October 2026, Article number 112913

Downloaded from a DSpace repository. https://dspace.org/